

---

**SYNTHESIS OF CdS NANOPARTICLES IN A MICROWAVE OVEN AND THEIR  
APPLICATION FOR BLOOD SERUM SENSING OF CARDIAC PATIENTS**

---

**By**

**EDMY J. FERRER TORRES**

A dissertation submitted in partial fulfillment  
of the requirements for the degree of

**DOCTOR IN PHILOSOPHY**

**In**

**APPLIED CHEMISTRY**

University of Puerto Rico

Mayaguez Campus

2010

Approved by:

\_\_\_\_\_  
Samuel P. Hernández Rivera, PhD  
Member, Graduate Committee

\_\_\_\_\_  
Date

\_\_\_\_\_  
Francis Patrón, PhD  
Member, Graduate Committee

\_\_\_\_\_  
Date

\_\_\_\_\_  
Jorge L. Rios Steiner, PhD  
Member, Graduate Committee

\_\_\_\_\_  
Date

\_\_\_\_\_  
Roberto Irizarry, PhD  
Member, Graduate Committee

\_\_\_\_\_  
Date

\_\_\_\_\_  
Miguel E. Castro Rosario, PhD  
President, Graduate Committee

\_\_\_\_\_  
Date

\_\_\_\_\_  
Arturo J. Hernández, PhD  
Representative of Graduate Studies

\_\_\_\_\_  
Date

\_\_\_\_\_  
Francis Patrón, PhD  
Chairperson of the Department

\_\_\_\_\_  
Date

## ABSTRACT

---

Nanoparticles include any type of particle up to 100 nm in size. Because of their properties, they play an important role in a wide variety of fields. We report here the formation of CdS nanoparticles from the microwave assisted reaction of  $\text{Cd}(\text{CH}_3\text{CO}_2)_2$  with DMSO. DMSO serves as the solvent and as a controlled source of sulfide ions to form  $(\text{CdS})_{1 \leq n \leq 5}$  clusters at the early stages of the process. The clusters grow into CdS nanoparticles, with diameters that range from 1.6 nm up to over 250 nm, with microwave heating time. The time dependence of the onset of light absorption and absorbance near the band edge are consistent with a concurrent nucleation and growth processes. The formation of clusters and nuclei and their subsequent reactions is controlled by turning on and off the energy supply consistent with an energy barrier to CdS nanostructures formation.

The use of sensors to improve health and our quality of life are just some of the applications that sensors have. Nanotechnology may represent a tool for the improvement in our quality of life by providing a platform for new sensors or sensing element components that can be integrated into functional sensors- to monitor chemicals closely related to health issues. Coronary heart disease is the leading cause of death for both men and women in USA. We present results on the evaluation of the response of CdS semiconductor nanoparticles in the serum of patients who have been evaluated for cardiac troponin. Our method results in an improvement in the detection limit compare with the Abbott method essay currently employed in clinical tests. Detection limits of the orders of a few nanograms were established in studies of the serum of three patients. This represents a factor of  $10^3$  compared to the Abbott clinical test.

## RESUMEN

---

Las nanopartículas incluyen cualquier tipo de partícula con un tamaño de hasta 100 nanómetros. Debido a sus propiedades, estas juegan un papel importante en una gran variedad de disciplinas. En este trabajo presentamos la formación de nano partículas de CdS al reaccionar  $\text{Cd}(\text{CH}_3\text{CO}_2)_2$  con DMSO en el microonda. DMSO funciona como el disolvente y la fuente controlada de iones de azufre para formar los aglomerados de (CdS) en las primeras etapas del proceso. Los aglomerados crecen en nanopartículas de CdS, en un rango de 1.6 hasta 250 nm de diámetro al exponerlas a tiempos de calentamiento en microonda. La dependencia del tiempo del “onset” de la absorción de la luz y la absorbencia son consistentes con un proceso de nucleación y crecimiento concurrente. La formación de los aglomerados, de los núcleos y de sus reacciones subsiguientes está controlada por el encendido y apagado de la fuente de energía, lo que es consistente con la presencia de una barrera energética que induce la formación de las nanoestructuras de CdS.

El uso de sensores para mejorar los cuidados de la salud y nuestra calidad de vida son solo algunos ejemplos de las aplicaciones que tienen los sensores. La nanotecnología representa una herramienta para mejorar nuestra calidad de vida y proveer una plataforma para el desarrollo de nuevos sensores o componentes de elementos de sensores que se pueden integrar a sensores funcionales para monitorear químicos relacionados a condiciones de la salud. Las enfermedades coronarias cardiacas son la mayor causa de muerte en los Estados Unidos. En este trabajo presento los resultados al evaluar la respuesta de nanopartículas semiconductoras de CdS al suero de los pacientes que fueron evaluados para troponina cardiaca. Nuestro método resulta en una mejora al límite de detección comparado con el ensayo de Abbott que actualmente se emplea en las pruebas clínicas. Límites de Detección en el orden de algunos nanogramos fueron establecidos para el suero de tres pacientes. Esto representa un factor de  $10^3$  comparado con la prueba clínica de Abbott.

© 2010 Edmy J. Ferrer Torres

---

---

I dedicate this dissertation to the person who supported and believed in me. The woman that taught me that in life we have to fight to obtain our dreams. She showed me to put every goal in God's hands, because nothing is impossible for Him. The woman that with her testimony gave me the strength to fight and never give up. In memory of the best mother of the world, Myrna E. Torres Rivas, a real example of strength and faith, I know that she would be happy to celebrate with me this achievement. I love you mom, thanks for giving the best of you and teach me to fight by my God's hand.

---

## AKNOWLEDGEMENTS

---

I want to thanks:

First God who gave me the strength to continue and help me every time.

My loving family: Joel Ruiz Martínez my husband, Alondra Z. Ruiz Ferrer, Paola J. Ferrer and Diego A. Ruiz Ferrer my kids, to my father Edgar O. Ferrer Torres, my brother Edgar O. Ferrer Torres and Grandparents Osvaldo Ferrer and Margarita Torres for their support and motivation.

My special friends who encourage me all time and support me, Margarita Suau my second mom, my best friend and sister María del Carmen Rodríguez and her husband Carlos Frontera, my sisters Raquel Feliciano, Iris Debra and Raquel Rodríguez.

My lab partners and friends Madeline S. León, Daniel Rivera, Miguel González and Eunice Mercado.

My advisor Dr. Miguel E. Castro Rosario and my graduate committee Dr. Francis Patrón, Dr. Jorge L. Rios Steiner, Dr. Samuel Hernández and Dr. Roberto Irizarry

Dr. López Garriga, Dr. Enrique Meléndez and Dr. Marcos De Jesús for lab facilities

Hewlette Packard for Internship opportunity

Prof. Lourdes Diaz, Lic. Eulalia Medina and the Science and Technology Department at the Interamerican University in Ponce for their support.

# TABLE OF CONTENT

---

Abstract	ii
Resumen	iii
Acknowledgements	vi
Table of Contents	vii
List of Figures	x
Table List	xii
Scheme List	xiii
1. CHAPTER 1	
Justification	1
2. CHAPTER 2	
Previous Work	4
3. CHAPTER 3	
Objectives	11
4. CHAPTER 4	12
Methodology	
5. CHAPTER 5	15
Synthesis of CdS nanoparticles by microwave irradiation	
5.1 Introduction	15
5.2 Experimental	18
5.3 Results and Discussion	19
5.4 CdS NP characterization	22
5.5 CdS Formation Mechanism	24

5.6 Theoretical Mechanism of cluster formation	26
5.7 CdS Nucleation and Growth	31
5.7.1 CdS Nucleation	34
5.7.2 Growth of CdS nanoparticles	35
5.8 Discussion	40
5.6 Conclusion	42
5.7 Acknowledgments	43
5.8 References	43

## 6. CHAPTER 6

### Fluorescence response of CdS nanoparticles to serum of cardiac patients

6.1 Introduction	47
6.1.1. Introduction to basic solid state physics	47
6.1.2. Quantum size effects	51
6.1.3. Sensing applications of nanoparticles in biological systems	55
6.1.4. Nanotechnology for sensing cardiac failure	59
6.2 Justification	60
6.3 General Background	61
6.4 Objective of proposed research	64
6.5 Methodology	65
6.6 Results and discussion	66
6.7 Acknowledgements	69
6.8 References	70

9. CHAPTER 7	72
Conclusion	
10. CHAPTER 8	73
Future Works	
11. CHAPTER 9	
General References	76
12. APPENDIX	
Appendix A	84

## LIST OF FIGURES

Figure		Page
5.1	CdS nanoparticles formation by the addition of the Cd(CH <sub>3</sub> CO <sub>2</sub> ) <sub>2</sub> to DMSO	21
5.2	Representative TEM images of 30 x 30 nm <sup>2</sup> areas obtained on deposit prepared from a 0.001g/mL Cd(CH <sub>3</sub> CO <sub>2</sub> ) <sub>2</sub> in DMSO solution exposed to microwave radiation for 150s and dispersed in ethanol.	23
5.3	Nanoparticles size distribution for 150s TEM image.	23
5.4	The absorption spectra of a diluted Cd(CH <sub>3</sub> CO <sub>2</sub> ) <sub>2</sub> in DMSO solution as a function of microwave exposure time. The insert illustrates the dependence of the absorption at 270, 400 and 500 nm on time.	26
5.5	The variation of the (CdS) <sub>n</sub> cluster energy on aggregation number n.	30
5.6	Absorption spectra of a 0.001 mg/mL Cd(CH <sub>3</sub> CO <sub>2</sub> ) <sub>2</sub> in DMSO solution as a function of time in the microwave.	33
5.7	The dependence of the absorbance at 400 nm on time for solutions with [Cd(CH <sub>3</sub> CO <sub>2</sub> ) <sub>2</sub> ] <sub>0</sub> of 0.0005 (triangles), 0.001 (squares) and 0.003 (circles) mg/mL.	35
5.8	Representation of the onset of light absorption as a function of heating time of 0.001 and 0.003 mg/ mL Cd(CH <sub>3</sub> CO <sub>2</sub> ) <sub>2</sub> in DMSO solutions, respectively.	37
5.9	The absorption spectra of the CdS NP prepared immediately and two months after their preparation, respectively. FESEM images of a CdS NP solution prepared from exposing the Cd(CH <sub>3</sub> CO <sub>2</sub> ) <sub>2</sub> in DMSO solution to microwave radiation for over 300 seconds.	39
5.10	EDAX mapping for FESEM image	40
6.1	The energy bands of metals, semiconductors and insulators. For insulators and semiconductors, the lower band is called the valence band and the higher band is called the conduction band. The lower energy band in metals is partially filled with electrons.	49

6.2	Structure of skeletal troponin complex	63
6.3	A model of the molecular arrangement of troponin (Tn), tropomyosin (Tm), and actin in the cardiac muscle thin filament.	64
	Human Blood Serum	
6.4		66
6.5	The fluorescence spectra of DMSO, the CdS nanoparticles in DMSO, the serum of patients with no detectable troponin (patient 1), and of a patient containing 1.8 mg/mL of troponin (patient 2).	68
6.6	Emission intensity of a concentration profile for 1.8mg troponin serum of cardiac patient. Addition of 30 $\mu$ L, 45 $\mu$ L, 60 $\mu$ L and 90 $\mu$ L to 1mL of a solution containing approximately $1.5 \times 10^{12}$ CdS nanoparticles were performed. Figure show the increase in emission intensity as a function of cardiac patient serum concentration.	69

## TABLE LIST

---

<b>Table</b>		<b>Page</b>
5.1	Predicted ground state HOMO-LUMO gap and relevant CIS wavelength dependent-oscillator strengths of optimized structures	31
6.1	Common Cardiac Biomarkers	62

## SCHEME LIST

---

SCHEME		Page
5.1	Cd(CH <sub>3</sub> CO <sub>2</sub> ) <sub>2</sub> and DMSO as precursors to Cd <sup>2+</sup> and S <sup>-2</sup> ions	16
5.2	The optimized structures of (CdS) <sub>n</sub> and (Cd <sub>n</sub> S <sub>n+1</sub> ) <sup>-2</sup> clusters	32
6.1	Charge transfer process between TNT and quantum dots	54

## CHAPTER 1: JUSTIFICATION

---

The Dictionary of the Spanish Royal Academy defines a sensor as a device that receives and responds to a signal or stimulus. It measures or detects a physical condition, most commonly, motion, heat or light, and converts the condition into an analog or digital representation. Over the past 20 years there has been a revolution in sensing capability due to advances in the development of microelectronics, which has allowed building sensors with multiple capabilities in devices of relatively small dimensions. The purpose of all sensors is to gather data regarding the physical world that will, in some way, be used to affect the control of the system.<sup>1</sup> Some sensors are integrated in closed-loop control systems that function largely in the absence of human intervention, allowing for their use in unsafe (hostile) environments.

The use of sensors for national security and health care improvement are just some of the applications that the sensors have. Coronary heart disease, on the other hand, is the leading cause of death for both men and women in the USA. Heart disease is caused by the narrowing of the coronary arteries that feed the heart. Like any muscle, the heart needs a constant supply of oxygen and nutrients, which are carried to it by the blood in the coronary arteries. When the coronary arteries become narrowed or clogged by cholesterol and fat deposits, a process known as atherosclerosis occurs. When not enough blood is supplied to the heart, the result is coronary heart disease (CHD). If there is not enough oxygen-carrying blood reaching the heart, you may experience a chest pain called angina. If the blood supply to a portion of the heart is completely cut off by total blockage of a coronary artery, the result is a heart attack. This is usually due to a sudden closure of an artery from a blood clot forming on top of previous narrowing<sup>3</sup>.

Since the 1900's, cardiovascular diseases have been the number one killer in USA every year. Around fifty seven percent of the men and sixty four percent of women that suffer sudden

death by cardiovascular diseases do not exhibit physical characteristics easily associated with heart failure. The cost of cardiovascular diseases in 1999 was about 286,500 thousands of million dollars, which trickles down onto consumers thru higher insurance premiums and expensive intensive health care services at hospitals.<sup>3</sup> Each year, about 1.1 million americans suffer a heart attack and about 460,000 of those heart attacks are fatal. Approximately half of those deaths occur within one hour of the start of symptoms and before the victim reaches the hospital.

Recent studies related to cardiovascular diseases show that Troponin I is an excellent biological marker for cardiovascular diseases. Troponin I is a protein released into the human blood stream after heart damage occurs and about five to six hours prior to a heart attack. Early troponin detection provides the best tool for the detection of coronary disease prior to a major heart attack. However, current methods for troponin detection are time consuming. Therefore the development of a real time sensor for troponin detection would be of great benefit.

Nanotechnology may present a tool for the improvement in our quality of life by providing a platform for novel sensors to monitor chemicals closely related to security and health issues. Nanoparticles, a unique subset of the broad field of nanotechnology, include any type of particle with at least one dimension a few nanometers in size. Nanoparticles play an important role in a wide variety of fields including advanced materials, pharmaceuticals, and are being explored for environmental detection and monitoring<sup>5</sup>. Engineered nanoparticles are intentionally designed and created with physical properties tailored to meet the needs of specific applications. They can be end products by themselves, as in the case of quantum dots or pharmaceutical drugs, or they can be components to be incorporated later in end products, such as carbon black in rubber products. Either way, the particle's physical properties are extremely important to their performance or the performance of any product into which they are ultimately incorporated.

Non-engineered nanoparticles, on the other hand, are unintentionally generated nanoparticles, such as atmospheric nanoparticles created during combustion. With non-engineered nanoparticles, physical properties also play an important role as they settle on whether or not ill effects will occur as a result of the presence of these particles.<sup>6</sup> Depending on the application of interest, nanoparticles may be known by a number of alternative and trade-specific names, including particulate matter, aerosols, colloids, nanocomposites, nanopowders, and nanoceramics. Some industries with engineered nanoparticles are pharmaceuticals, performance chemicals, chemical and mechanical polishing, quantum dots, biodetection and labeling, ceramics, food products and cosmetics. Non-engineered particles are used in environmental detection, environmental monitoring and controlled environments.

## CHAPTER 2: PREVIOUS WORK

---

Understanding the properties and methods of preparation of nanoparticles we can contribute to the development of sensors that improve our quality of life. The most common methods for nanoparticle preparation include sonochemical synthesis, hydrothermal synthesis and chemical reactions. Several researchers focused their studies on these methods<sup>3-10</sup>. These methods present some limitations. For example to stop nanoparticle growth they need to adsorb organic surfactants or inorganic ligands that hinder growth. This results in poor purity and limits field use. Lack of knowledge of preparation history of commercially available limits their use in basic research.

Liang Li, and Junjie Zhu studied a new approach for nanoparticles preparation by using microwave irradiation<sup>11-12</sup>. The method results in a very simple fast reaction and they obtained high quality nanoparticles. Since nanomaterials have unique chemical, physical, and mechanical properties, they can be used for a wide variety of applications. Nanoscale materials have optical properties that differ substantially from their bulk counterparts. Gold nanoparticles present fascinating behavior such as their multiple types of assembly, its individual particles behavior, size-related electronic, magnetic and optical properties (quantum size effect) and their application in catalysis and biology.<sup>1, 13</sup> Prashant V. Kamat focused on the photophysical, photochemical and photocatalytic aspects of metal nanoparticles. Metal nanoparticles, such as gold and silver, exhibit noticeable photoactivity under UV-visible irradiation. Nanosize semiconductor materials have band gaps that are strongly size dependent, increasing with a decrease in cluster size, due to the quantum confinement effects. These nanoclusters exhibit photoluminescence (PL) that shifts to higher energies with decreasing cluster

size<sup>1</sup>. In this work they focused on PL from gold colloids form in water by sodium citrate reduction. Strong size dependent photoluminescence from solutions of gold nanoclusters was observed. For this experiment the emission detector was set to 440 nm peak of the PL and the excitation wavelength was then scanned over the range 190-400 nm. It was found that the position and shape of the PL peak is almost independent of the excitation wavelength within this excitation range. They noted that on a cluster basis, the strength of this PL peak is comparable to many semiconductor nanoclusters, for example CdS or MoS<sub>2</sub>. The 15 nm Au Clusters do not show luminescence at any excitation wavelength, demonstrating that PL occurs only for small nanoclusters (2.5 nm, 5 nm). The etching of larger nonluminescent gold colloids using KCN results in smaller luminescent clusters.

Recently, one and multicolor luminescent blinking from a variety of noble-metal nanostructures upon laser illumination was observed. Chris D. Gedes, et. al. studied the luminescent blinking of gold nanoparticles and previously studied silver nanoparticles<sup>14</sup>. The results suggest a new class of metallic probes, based on intrinsic metal luminescence with several advantages over conventional organic fluorophores such enhanced photostability, higher luminescent intensity, tunable emission wavelengths and the possibilities for a variety of functional surface chemistries. Their findings show some notable and attractive differences between gold and silver nanostructures in their individual luminescence properties. Silver nanostructures deposited on glass slides show a time dependent activation and subsequent luminescent blinking, with multicolor blinking, differing in both intensity and location, also dependent on the type of structure and irradiance used. They observed that silver fractal like structures were highly emissive and could be photoactivated at much lower irradiance, typically less than 30 W/cm<sup>2</sup>, compared to glass-coated silver islands films and colloids, where silver

islands were found to be least emissive under similar experimental conditions. Higher irradiances are required to observe gold colloid luminescence, typically  $\text{kW}/\text{cm}^2$ . Gold colloids have been observed to blink, in contrast to silver. The color and emission spectra of the blinking spots remained the same with continuous illumination. This interesting difference suggests the use of silver nanostructures as probes for multicolor applications. The control of the nanoscale optical properties of silver nanostructures has led to nanophotonic devices ranging from nanosensors to waveguides, as well in a wide variety of biotechnology applications. These results also suggest the use of gold colloid cluster emission in nanotechnology and for optical probes in biotechnology and medical imaging<sup>14</sup>.

The most important property of semiconductor nanocrystals is the substantial change in optical properties as a function of size. As size is reduced, the electronic excitations shift to higher energy, and the oscillator strength is concentrated into just a few transitions. These phenomena of quantum confinement arise as a result of changes in the density of electronic states and can be understood by considering the relation between position and momentum in free and confined particles. For a free particle, or a particle in the periodic potential of an extended solid, the energy and the crystal momentum can both be precisely defined, whereas the position cannot. For a localized particle, the energy may still be well defined, but since the uncertainty in position decreases, the momentum is no longer well defined. The discrete energy eigenfunctions of the particle may then be viewed as superpositions of bulk momentum states. Given the relation between energy and momentum in the bulk solid, one can see how a series of nearby transitions occurring at slightly different energies in the bulk will be compressed by quantum confinement into a single, intense transition in a quantum dot<sup>13</sup>.

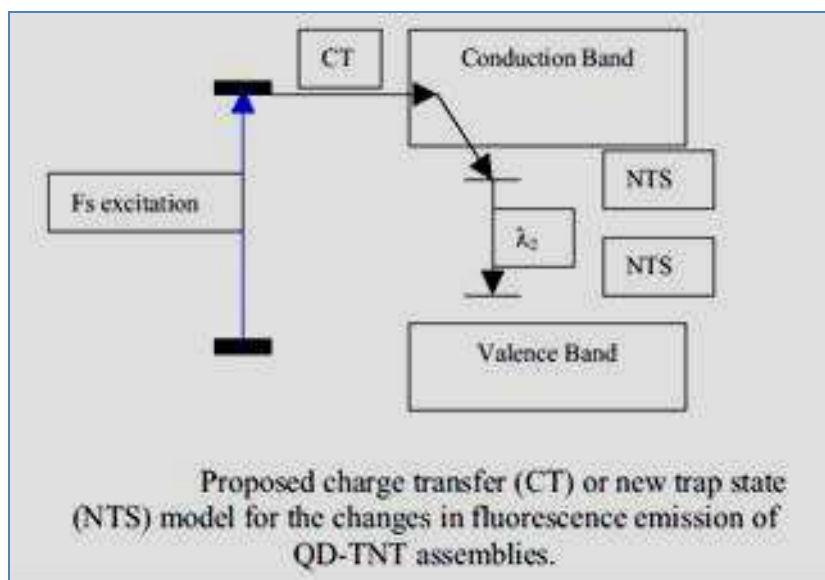
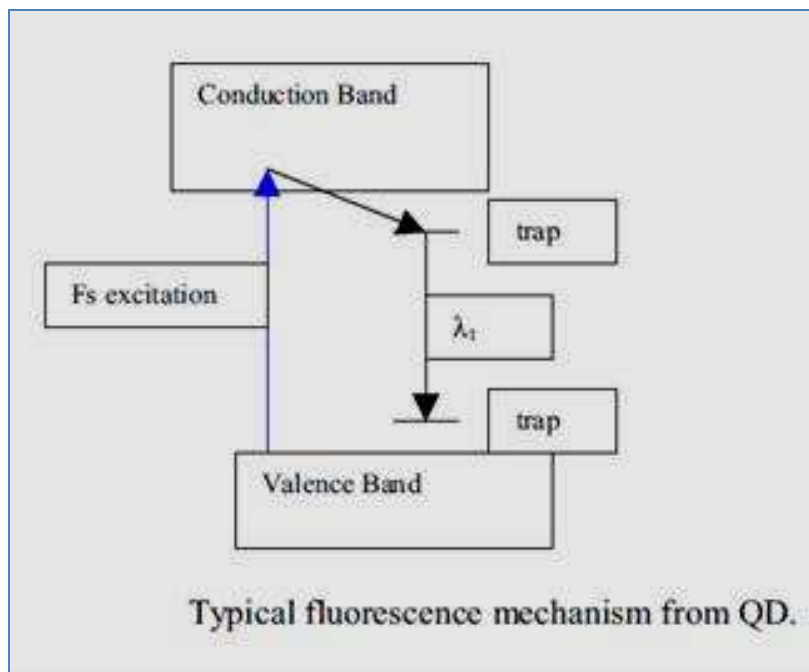
J. J. Mock et. al. presents a systematic study of the effect of size and shape on the spectral response of individual silver nanoparticles<sup>15</sup>. They found that specific geometrical shapes give distinct spectral responses. The relationship between the geometrical shape of an individual particle and its plasmon resonant spectral response has only recently been studied with modern optical microscopy techniques. In this study, they combine the use of an optimized optical detection technique with high-resolution transmission electron microscopy (TEM) analysis for the systematic investigation of the effects of shape on the surface plasmon resonance of individual silver colloidal nanoparticles. Nanoparticles of various shapes and sizes, from approximately 40 to 120 nm, having colors ranging from violet 400 nm to red 700 nm , were characterized. They used several experimental techniques to precisely correlate the optical spectrum of individual silver nanoparticles to their geometrical shapes. Although 40–120 nm in size, the plasmon resonant effect in silver nanoparticles makes them easily detectable in the visible spectrum using standard far-field optics. They assigned a size to each particle from the TEM images, taken with the e-beam normal to the sample, by comparing a characteristic dimension to the TEM calibration bar. In order to investigate the relationship between the size, shape, and color of silver nanoparticles in more detail, they made particles of various sizes by preparing several colloidal solutions, which differed in the amount of silver enhancer added in the sample preparation method. They found that with increased particle size the corresponding spectra are red shifted. In addition, a simple heat treatment can modify a particle shape, resulting in a change in its optical plasmon resonant properties. Such classification and tuning of the shape and optical properties of individual silver nanoparticles makes them excellent candidates for further applications in near field optical microscopy and biological assays.

The small size results in new quantum phenomena that yield some extraordinary bonuses. Material properties change dramatically because quantum effects arise from the confinement of electrons and "holes" in the material. Size changes other material properties, such as the electrical and nonlinear optical properties of a material, making them very different from those of the material's bulk form. The quantum size effect is involved when the Broglie wavelength of the valence electrons is of the same order as the size of the particle itself. Then, the particles behave electronically as zero dimensional quantum dots or quantum boxes driven by quantum mechanics rules. If a dot is excited, the smaller the dot, the higher the energy and intensity of its emitted light. Hence, these very small, semiconducting quantum dots are gateways to an enormous array of possible applications and new technologies. Gammon, Daniel et. al., made optical studies of single quantum dots<sup>16</sup>. Quantum dots measure between 1-100 nm, are semiconductor structures in which the electron wavefunction is confined in all three dimensions by the potential energy barriers that form quantum dot boundaries. A quantum dot, QD, electronic response, like that of a single atom, is manifest in its discrete energy spectrum, which appears when electron-hole pairs are excited. Although the wavefunction of a QD electron, and its corresponding hole, extends over many thousand lattice atoms, the pair termed an exciton behaves in a quantized and coherent fashion. The coherence is relatively easy to detect and control optically. Another attractive property of the quantum dot is that their size, shape and composition can all be tailored to create a variety of desired properties.

Many types of quantum dots materials have been developed, electrostatic and epitaxial QDs for example. Researchers have made a flurry of new and direct observations of fine structure splittings, hyperfine shifts and so on. These splitting contain the details of spin interactions and other quantum properties. The interaction of energy between excitons leads to the possibility of

generating single photons on demand. A strong laser pulse can create a state of many excitons, each of which has a different energy. But only one photon is emitted at the single exciton transition energy. A narrow bandpass filter tuned to the single exciton emission line can therefore be used to realize a solid-state source of single photons. One of the goals driving QD research, and nanostructure research is the creation of complex nanomaterials with customized properties.

S.Nieto et. al. studied nanoscaled sensing for quantum dots fluorescence quenching for nitrated explosives<sup>17</sup>. Nanoscaled semiconductors have the potential to be employed in trace explosive detection. They reported the effect of 2,4,6 trinitrotoluene on the fluorescence emission of zinc sulfide (ZnS) protected cadmium selenide (CdSe) quantum particles. The fluorescence was excited off resonance with respect to the quantum dots, but close to the absorption band edge of the TNT. The results presented were consistent with the extensive quenching and a change in fluorescence emission of QD by TNT. They found that the second wavelength (quantum dots plus TNT) was distinct from the emission wavelength ( $\lambda_1$ ) in the absence of the TNT. One of the important contributions of this work is the observation that the relative peak area decrease with the amount of added TNT to the solution. The measurements showed that the fluorescence intensity was proportional to the concentration of the quantum dots in solution. The fluorescence of the QDs is quenched by the added TNT. They found that the TNT doesn't have an effect on the size of the QD. The schemes below show the mechanism of charge transfer between TNT and the QD that they proposed.



They proposed a charge transfer process between TNT and quantum dots and/or the involvement of the new trap states (NTS) in the fluorescence emission of the dots. In chapter 6, we used an extension of this concept to detect cardiac troponin in the samples of the blood serum of real patients.

## CHAPTER 3: OBJECTIVES

---

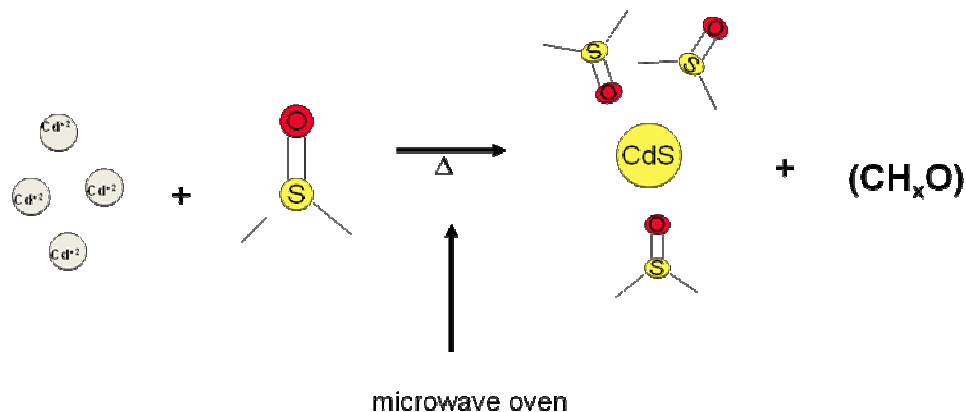
The objectives of this dissertation are the following:

1. To develop a new method for the facile synthesis of CdS fluorescent nanoparticles that can add to the battery of methods available and can facilitate their use as sensor or sensor elements.
2. To examine and make a critical judgment of the use of CdS NP for sensing cardiac troponin in patients.

## CHAPTER 4: GENERAL METHODOLOGY

---

### A. Synthesis of Nanoparticles



Our method for nanoparticle synthesis controls the NP size without adding capping agents using microwave heating. DMSO (HPLC grade Aldrich, 99.9%) was further purified by distillation to remove traces of water. Cadmium acetate dehydrate  $\text{Cd}(\text{CH}_3\text{CO}_2)_2$  was purchased from SIGMA ALDRICH (99%) and used without further purification. The desired amounts of the solid used for the solutions employed here were determined in a Metler Toledo AT 20 microbalance. The DMSO served as the solvent and source of sulfur to form the CdS nanoparticles in the experiments described here. A commercial microwave oven operating at 1500 Watts and 20 Hz and a microwave digestive system operating at 100 watts and 300 Hz were employed for the CdS NP synthesis. The solutions were exposed to microwave radiation at ten seconds (10) intervals until the desired time was achieved. More details on time exposure are discussed in chapter 5.

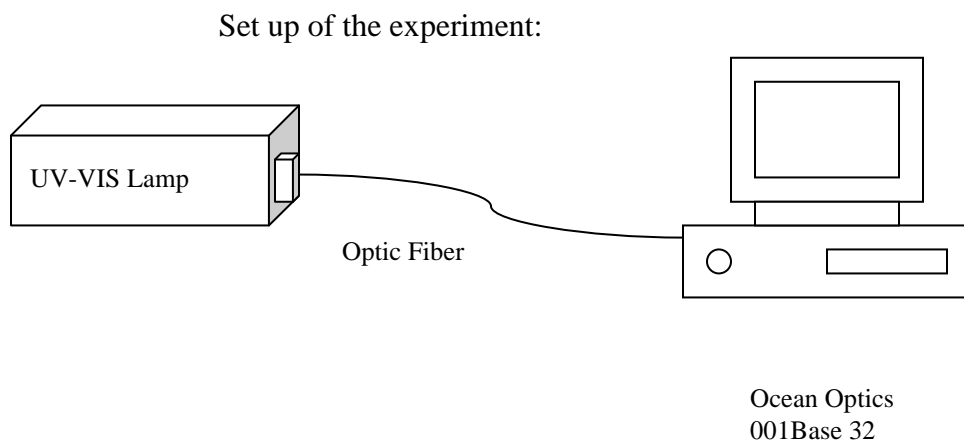
### B. Characterization of Nanoparticles

The characterization of the nanoparticles is essential. It's important to us determines the size of the nanoparticles. These characteristics cause a variation in the optical properties. A

relation between the wavelength of UV absorption and the size of the nanoparticle was established in previous works<sup>18</sup>. More details of this relation is explained in chapter 5.

### 1. Optical Studies

UV absorption spectroscopy was performed with a PC 2000 Ocean Optics UV-VIS spectrograph coupled to a high pressure deuterium lamp.



Emission measurements were performed in a Shimadzu RF 5301 Spectrofluorophotometer.

3. For shape and size determination Transmission electron microscopy measurements were performed in a JEOL 2010 TEM operated at an acceleration voltage of 140 kV. Negatives of the micrographs were processed using standard techniques and scanned with an EPSON Perfection V750 PRO scanner and stored in the computer for further analysis. Field emission scanning electron microscopy measurements were performed in a Philips FEG-SEM XL30 system.

C) Studies of the interaction of nanoparticles with cardiac troponin serum were done by using absorption and emission studies. We focused in the changes in the optical properties of the nanoparticles. In chapter 6, a more detail explanation is provided.

## CHAPTER 5: SYNTHESIS OF CdS NANOPARTICLES IN THE MICROWAVE<sup>24</sup>

---

### ABSTRACT

We report here the formation of CdS NP from the microwave assisted reaction of Cd(CH<sub>3</sub>CO<sub>2</sub>)<sub>2</sub> with DMSO. DMSO serves as the solvent and as a controlled source of sulfide ions to form (CdS)<sub>1≤n≤5</sub> clusters at the early stages of the process. The clusters grow into CdS nanoparticles, with diameters that range from 1.6 nm up to over 250 nm, with microwave heating. The time dependence of the onset of light absorption and absorbance are consistent with a concurrent nucleation and growth processes. The formation of clusters and nuclei and their subsequent reactions is controlled by turning on and off the energy supply consistent with an energy barrier to CdS nanostructures formation.

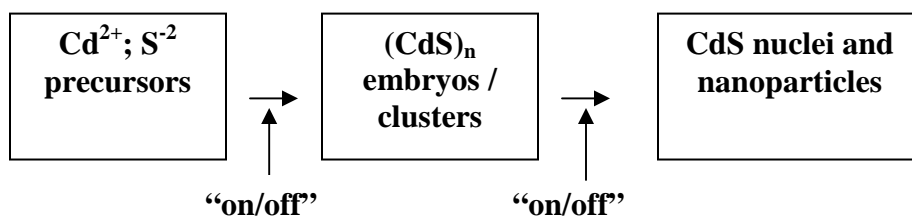
### 5.1 Introduction.

Cadmium sulfide nanoparticles (CdS NP) have interesting size dependent optical and electronic properties. CdS NP synthesis has been the subject of several studies due to their potential applications in sensing and solar cells.<sup>1</sup> The observation of quantum confinement effects in CdS NP in the size range of 2 to 8 nm has motivated numerous studies focused on selective size and morphology control. Knowledge of the elementary steps associated with nucleation and growth is a central and fundamental question in developing synthetic strategies to obtain CdS with the desired size and morphology. The methods for CdS NP synthesis reported to date include the use of wet chemical approaches, vapor deposition and molecular beam epitaxy.<sup>1</sup>

Capping agents have been used to limit particle size growth. Micelles, reverse micelles, porous glasses and the cavities of zeolites have served to tailor CdS NP particle size.<sup>2,3,4</sup> These methods, while effective to the size selective preparation, present limitations to use of CdS NP in sensing

applications, where an active surface is required. In this regard, physical methods that supply energy to initiate nucleation and growth are very attractive to the preparation of NP. Reactions initiated in the high temperature environment of acoustic cavities and under microwave irradiation as well as the selective photochemical decomposition of precursors are attractive approaches to control the extent of nucleation and growth in NP synthesis.<sup>5-11</sup> Microwave assisted reactions have gained popularity over conventional wet chemical approaches due to ease of use and availability. The molecular level heating leads to homogeneous and faster thermal reactions than those performed in other methods.<sup>12</sup>

The use of microwave radiation for the synthesis of CdS NPs has been the subject of a few recent works. These previous works focused on the use of thioacetamide as the source of the sulfide ions. Martinez et.al.<sup>13</sup> performed the synthesis of CdS nanoparticles from the reaction of CdCl<sub>2</sub> and thioacetamide using microwave irradiation. They found a direct relationship between the pH of the solution and the NPs size. Singh and coworkers<sup>5</sup> used a combination of sonochemical and microwave methods for the synthesis of CdS powders. These authors used sonochemistry to generate the sulfide ions from thioacetamide followed by microwave radiation to form the final CdS NP.<sup>5</sup> Zhu and coworkers<sup>14</sup>, on the other hand, exposed a mixture of thioacetamide and CdCl<sub>2</sub> to microwave radiation to prepare CdS.



Scheme 5.1: Cd(CH<sub>3</sub>CO<sub>2</sub>)<sub>2</sub> and DMSO serve as precursors to Cd<sup>2+</sup> and S<sup>2-</sup> ions. These ions react upon heating in the microwave to form embryos or clusters in the initial stages of the CdS NP synthesis. These embryos or clusters form CdS nuclei which further react to form CdS nanoparticles.

The formation of nanoparticles may be qualitatively discussed in the context of classic nucleation and growth theory. As illustrated in Scheme 5.1, the initial reactions of the precursors result in the formation of clusters or embryos. These embryos must overcome an energy barrier to form stable nuclei. The total change in free energy,  $\Delta G$ , for the nucleation process is a delicate balance between the surface free energy,  $\gamma$ , and the difference in chemical potential ( $\Delta\mu$ ) between the embryonic and nucleation phases. While the formation of chemical bonds generally results in a decrease in  $\Delta\mu$ , the growth in embryo or cluster size results in an increase in  $\gamma$ : the balance among these terms results in the appearance of a maximum in  $\Delta G$  with cluster size.<sup>15-18</sup> The presence of energy barrier(s) along the sequence of reactions leading to nucleation requires the supply of energy to move forward from the precursors to the final CdS NP. If the energy is supplied and suddenly cut off during a given step, it is possible to isolate those stable chemical species that are trapped between the steps of the process. In this regard, the molecular level heating associated with the use of microwaves to heat up chemical reactions offers the unique advantage to turn “on” and “off” chemical process and trap the different clusters or nuclei that serve as intermediates to nanoparticle synthesis.

We report here on the preparation of CdS NPs and  $(\text{CdS})_n$  clusters using  $\text{Cd}(\text{CH}_3\text{CO}_2)_2$  and DMSO as the source of cadmium and sulfide ions, respectively. Solutions of  $\text{Cd}(\text{CH}_3\text{CO}_2)_2$  in DMSO were heated in a microwave oven and studied as a function of exposure time and initial concentration. Turning “on” the microwave allows the reactants to form cadmium sulfide clusters and nanoparticles. Turning “off” the microwave allows characterization of those clusters that serve as embryos to form nuclei and larger nanoparticles using standard spectroscopic measurements under steady conditions. The optical properties of the CdS particles were established with UV-visible absorption and emission spectroscopy. Transmission electron

microscopy (TEM) and field emission scanning electron microscopy (FE SEM) measurements were performed to characterize particle size and morphology. Formation of CdS monomers and  $(\text{CdS})_n$  clusters ( $2 \leq n \leq 5$ ) formed at the early stages of the reaction between  $\text{Cd}^{+2}$  ions and DMSO is established by measurements of the light absorbed below 300 nm. Theoretical calculations at the DFT/B3LYP/DGDZVP level of theory indicate that there is a barrier to the formation of the  $(\text{CdS})_4$  cluster, which is taken as a central factor in the accumulation of  $(\text{CdS})_n$  clusters with  $n \leq 3$  and open the opportunity for the formation of nonstoichiometric cadmium sulfide clusters. These clusters or embryos further react upon heating in the microwave to form CdS nuclei and nanoparticles. Analysis of the onset of light absorption and absorption near the band edge at 400 nm is consistent with simultaneous nucleation and growths. The extent of the nucleation and growth is controlled by the supply of sulfide ions from the reactions of DMSO and cadmium ions during exposure to microwave radiation.

## **5.2 Experimental.**

DMSO (HPLC grade Aldrich, 99.9%) was further purified by distillation to remove traces of water. Cadmium acetate dehydrate  $\text{Cd}(\text{CH}_3\text{CO}_2)_2$  was purchased from SIGMA ALDRICH (99%) and used without further purification. The desired amounts of the solid used for the solutions employed here were determined in a Metler Toledo AT 20 microbalance. The DMSO served as the solvent and source of sulfur to form the CdS nanoparticles in the experiments described here. A commercial microwave oven operating at 1500 Watts and 20 Hz or a microwave digestive system operating at 100 watts and 300 Hz were employed for the CdS NP synthesis. The solutions were exposed to microwave radiation in intervals of ten seconds (10) until the desired time was achieved. UV absorption spectroscopy measurements were performed with a PC 2000 Ocean Optics UV-VIS spectrograph coupled to a high pressure deuterium lamp.

Transmission electron microscopy measurements were performed in a JEOL 2010 TEM operated at an acceleration voltage of 140 kV. Negatives of the micrographs were processed using standard techniques and scanned with an EPSON Perfection V750 PRO scanner and stored in the computer for further analysis. Field emission scanning electron microscopy measurements were performed in a Philips FEG-SEM XL30 system.

### **5.3 Results and Discussion.**

#### **CdS NP Synthesis: UV-Visible Absorption and Fluorescence Measurements.**

$\text{Cd}(\text{CH}_3\text{CO}_2)_2$  was used as a convenient source of  $\text{Cd}^{+2}$  ions to form the CdS NP in dimethylsulfoxide (DMSO).<sup>19-20</sup> The addition of  $\text{Cd}(\text{CH}_3\text{CO}_2)_2$  to 20 mL of DMSO resulted in the formation of a clear solution. A yellow solution is formed when the mixture is placed in the microwave oven for time periods longer than 90 seconds: the yellow color becomes more noticeable and intense when the solution is placed in the microwave for longer times. UV visible absorption spectra of the solutions are displayed on the left hand side of figure 5.1. The UV visible absorption spectra of  $\text{Cd}(\text{CH}_3\text{CO}_2)_2$  in DMSO solutions exposed to microwave radiation are consistent with the formation CdS NP.<sup>1-4</sup>

Alky thiols are proposed to play a central role in the formation of CdS NP from the microwave assisted reaction of thioacetamide with  $\text{CdCl}_2$ .<sup>13</sup> Alkyl thiols are also known to be important products of the microwave decomposition of DMSO.<sup>13</sup> If the  $\text{Cd}(\text{CH}_3\text{CO}_2)_2$  is added to DMSO that has been previously placed in the microwave oven for 200 seconds, the color of the solution remains clear and no absorption features that can be attributed to CdS NP are observed in the absorption spectra. The addition of the  $\text{Cd}(\text{CH}_3\text{CO}_2)_2$  to a solution containing 0.011g/mL of 1-hexadecanethiol in DMSO failed to form a colored solution. Controlled experiments with a solution of  $\text{AgNO}_3$  in DMSO were also performed. Bands characteristic of  $\text{Ag}_2\text{S}$  nanoparticles

in the UV-visible absorption spectrum of  $\text{AgNO}_3$  in DMSO solutions exposed to microwave heating for up to 200 seconds were searched for, but not observed. These observations lead us to conclude that formation of CdS NP requires exposure of a solution containing both components to microwave radiation.

The CdS NP prepared by the method described here exhibit strong fluorescence. The emission spectrum of the CdS NP prepared by exposing a 0.002 g/mL solution to the microwave radiation for 150 seconds is also displayed on figure 5.1. The excitation wavelength is 340 nm. The CdS NP exhibited a weak fluorescence band around 400 nm and a stronger fluorescence band between 460 and 600 nm with a peak centered at about 520 nm. The fluorescence bands appear in a region of the spectrum similar to that reported for CdS NP prepared by other methods.<sup>8-9</sup> Excitonic recombination and trapped state emission contribute to the fluorescence in CdS NP. Excitonic recombination is usually sharper and is observed at shorter wavelengths than trap recombination. Excitonic recombination of photoexcited electrons with holes in the valence band of CdS has been observed between 400 and 450 nm: the band around 380 nm is attributed to excitonic emission. The peak centered at 520 nm, on the other hand, is attributed to trapped state emission. The band edge in these particles is around 500 nm. Since the method employed for the synthesis of the CdS NP used here requires a reaction between the sulfur provided by the solvent molecules and the  $\text{Cd}^{+2}$ , it is very likely that the CdS NP have ionic vacancies which may serve as shallow trap states, resulting in the broad emission band at 500 nm.

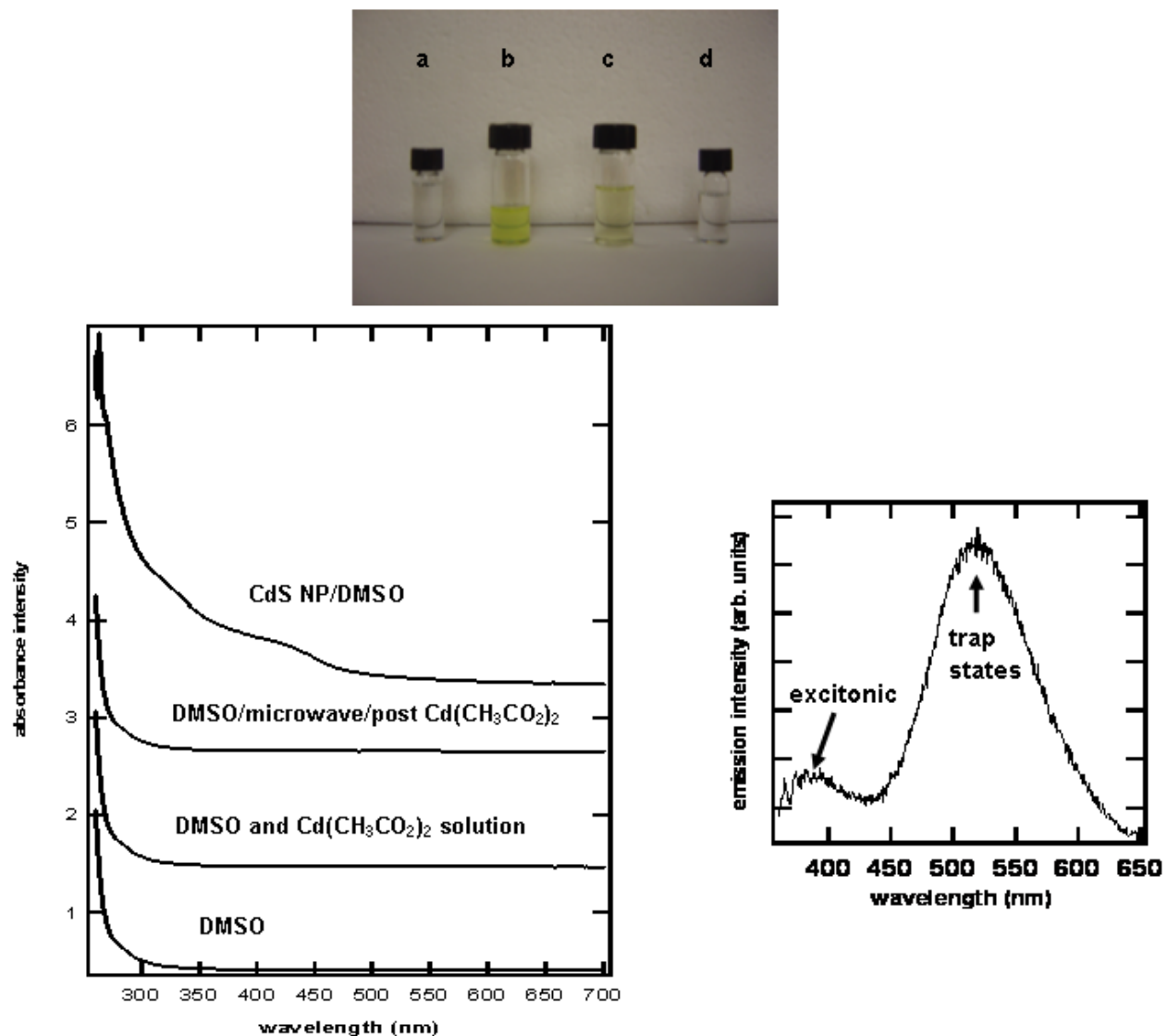


Figure 5.1: The clear and colored  $\text{Cd}(\text{CH}_3\text{CO}_2)_2$  in DMSO solutions formed (a) immediately after the addition of  $\text{Cd}(\text{CH}_3\text{CO}_2)_2$  to the DMSO, (b) and (c) after the solution is exposed to microwave radiation for 150 and 90 seconds, respectively. The picture obtained after the  $\text{Cd}(\text{CH}_3\text{CO}_2)_2$  is added to DMSO that has been exposed to microwave radiation for over 200 seconds is labeled 'd'. The figure at the bottom of the page illustrates the UV-visible spectra of, from top to bottom, (a) the DMSO employed for the measurements, (b) the solution of  $\text{Cd}(\text{CH}_3\text{CO}_2)_2$  in DMSO, (c) the solution formed upon addition of the  $\text{Cd}(\text{CH}_3\text{CO}_2)_2$  to DMSO that has been previously exposed to microwave radiation for 200 seconds and (d) the CdS NP prepared upon exposing the  $\text{Cd}(\text{CH}_3\text{CO}_2)_2$  in DMSO solution to microwave radiation. The emission spectra of CdS NP formed upon exposure of a 0.002g/mL  $\text{Cd}(\text{CH}_3\text{CO}_2)_2$  in DMSO solution to microwave radiation is illustrated on the lower right hand of the figure.

#### 5.4 CdS NP Characterization: Transmission Electron Microscopy Measurements.

TEM measurements were performed with the purpose of establishing that CdS nanoparticles are formed upon exposure of the  $\text{Cd}(\text{CH}_3\text{CO}_2)_2$  in DMSO solution to microwave heating. Representative TEM images on a deposit prepared from samples obtained after a 0.001 g/mL solution is warmed in the microwave oven for about 150 seconds are displayed on figure 5.2(a) and a closer view of a selected area is showed in figure 5.2(b). The images were obtained on a deposit prepared by dispersing a few microliters of the CdS in DMSO solution in a drop of ethanol on a carbon coated grid. Selected area electron diffraction (SAED) is illustrated in figure 5.2 (c). The spacing in the pattern of rings observed is consistent with previous reports for CdS NP prepared by other methods. The TEM images displayed in figure 5.2 (a) and 5.2(b) are consistent with the formation of CdS nanoparticles in the size ranges of 2 to 6 nm. In a few cases the particles arranged into islands with a diameter between 25 to 30 nm. The particle size distribution obtained from quantitative measurements on several areas of the sample examined is displayed on figure 5.3. The particles have a very narrow distribution with diameters between 1.5 and 6 nm. The average diameter of the CdS NP prepared as described here is  $(1.6 \pm 0.3)$  nm.

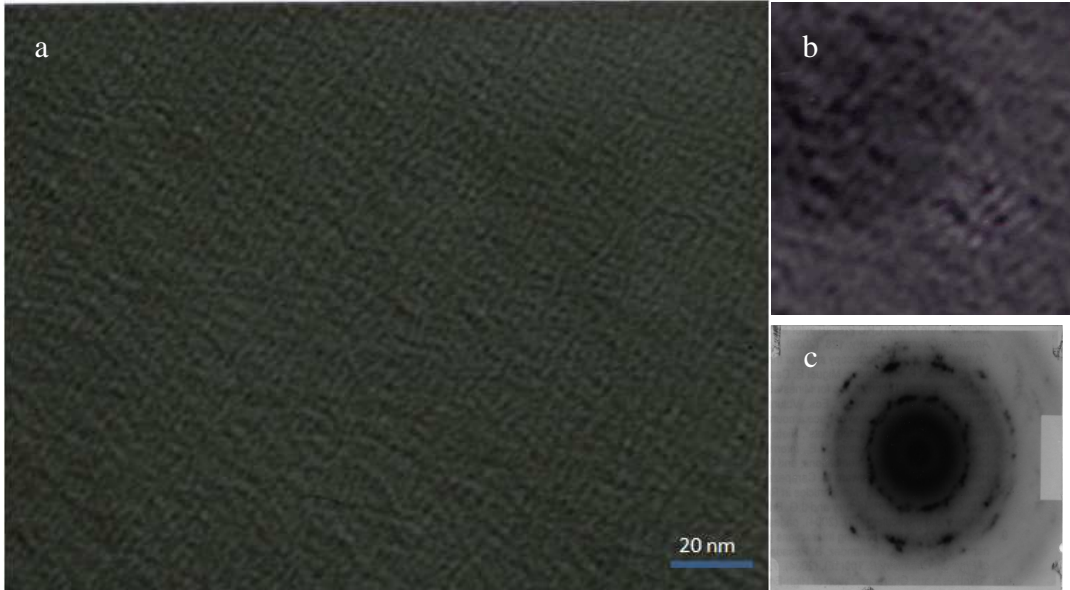


Figure 5.2: Representative TEM images of  $30 \times 30 \text{ nm}^2$  areas obtained on deposit prepared from a  $0.001 \text{ g/mL Cd}(\text{CH}_3\text{CO}_2)_2$  in DMSO solution exposed to microwave radiation for 150s and dispersed in ethanol.

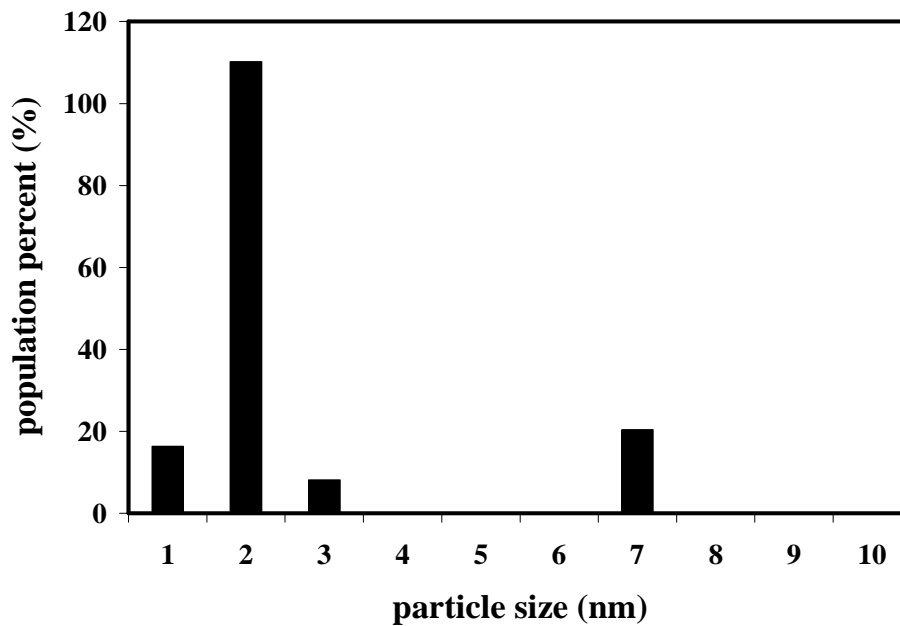


Figure 5.3: Nanoparticles size distribution for 150s TEM image.

## 5.5 CdS NP Formation Mechanism

### 5.5.1 Formation of (CdS)<sub>n</sub> Clusters in Diluted Solutions.

The reaction of the solvent molecules with Cd(CH<sub>3</sub>CO<sub>2</sub>)<sub>2</sub> upon heating the solution in the microwave initiates the sequence of reactions to form CdS NP:



The supply of sulfide ions from the initial reaction between DMSO and the Cd<sup>+2</sup> ions while heating in the microwave is required to form the clusters. Recent experimental work by Zeng and coworkers<sup>21</sup> have established the formation of (CdS)<sub>n</sub> clusters with n=1,2,3,4 and 5 in the synthesis of CdS NP under conditions of a limited supply of Cd<sup>+2</sup> ions. These clusters absorb exclusively UV light, between 230 and 285 nm. Theoretical calculations performed by the above authors on naked CdS clusters show an increase in the HOMO-LUMO gap with increasing aggregation number from n=1 (monomer) to n=5. The HOMO-LUMO gap is predicted to decrease to between 3 and 3.5 eV when the aggregation number increases to n=6.<sup>21</sup> Frenzel, Joswig and Seifert, on the other hand, have reported on the optical transitions of CdS clusters capped with S-H groups. The transition that requires the lowest energy in clusters containing between 1 and 4 Cd ions are predicted to occur between 5 and 4 eV, well into the UV region, consistent with the experimental results presented by Zeng and coworkers.

UV-visible absorption measurements were performed in diluted Cd(CH<sub>3</sub>CO<sub>2</sub>)<sub>2</sub> solutions exposed to microwave radiation for short periods of times with the purpose of establishing the formation of (CdS)<sub>n</sub> clusters in the microwave assisted synthesis of CdS NP. Representative UV-visible absorption spectra of a 0.0005 mg/mL Cd(CH<sub>3</sub>CO<sub>2</sub>)<sub>2</sub> in DMSO solution as a function of

exposure time in the microwave are displayed in figure 5.4. A band between 250 and 300 nm is the only feature observed in the UV-visible spectrum of diluted samples exposed to microwave heating for times shorter than 30 seconds. A band around 500 nm is observed when the sample is exposed to microwave heating for times longer than 50 s. The shape and wavelength in the UV region at which the bands are observed are in agreement with the results of Zeng for  $(\text{CdS})_n$  clusters with  $n=1$  to 5 and the theoretical work discussed in the previous paragraph. We therefore attribute the bands between 250 and 300 nm to the formation of  $(\text{CdS})_n$  clusters with aggregation numbers between 1 and 5. Samples containing these clusters exhibited a remarkable stability toward the formation of particles: we were able to reproduce their spectra quantitatively several days after the initial measurement. Further increase in microwave heating time of the  $\text{Cd}(\text{CH}_3\text{CO}_2)_2$  in DMSO solution results in spectra that resemble those obtained for larger initial  $\text{Cd}(\text{CH}_3\text{CO}_2)_2$  concentrations, with the edge around 400 nm and a long tail that results from overlapping CdS NP absorption edge and the 500 nm band. The inset in figure 5.4 compares the absorbance of the bands observed in the UV-visible measurements. The open circles in the insert of figure 5.4 represent the absorption at 270 nm. The absorption at 270 nm increases with heating time in the microwave oven. The open triangles and squares in the insert represent the absorbance at 400 and 500 nm, respectively. The absorbance at 400 and 500 nm start to increase around 50 seconds after the start of the reaction, indicating that there is an induction period for the formation of structures larger than the  $(\text{CdS})_{1-5}$  clusters. The absorbance at 500 nm saturates while the absorbance at 400 nm continues to increase in the time range studied. The absorbance at 400 nm results from the formation of CdS nuclei and NP. We are lead to the conclusion that the species responsible for the absorption of light at 500 nm are not further involved in nucleation reactions.

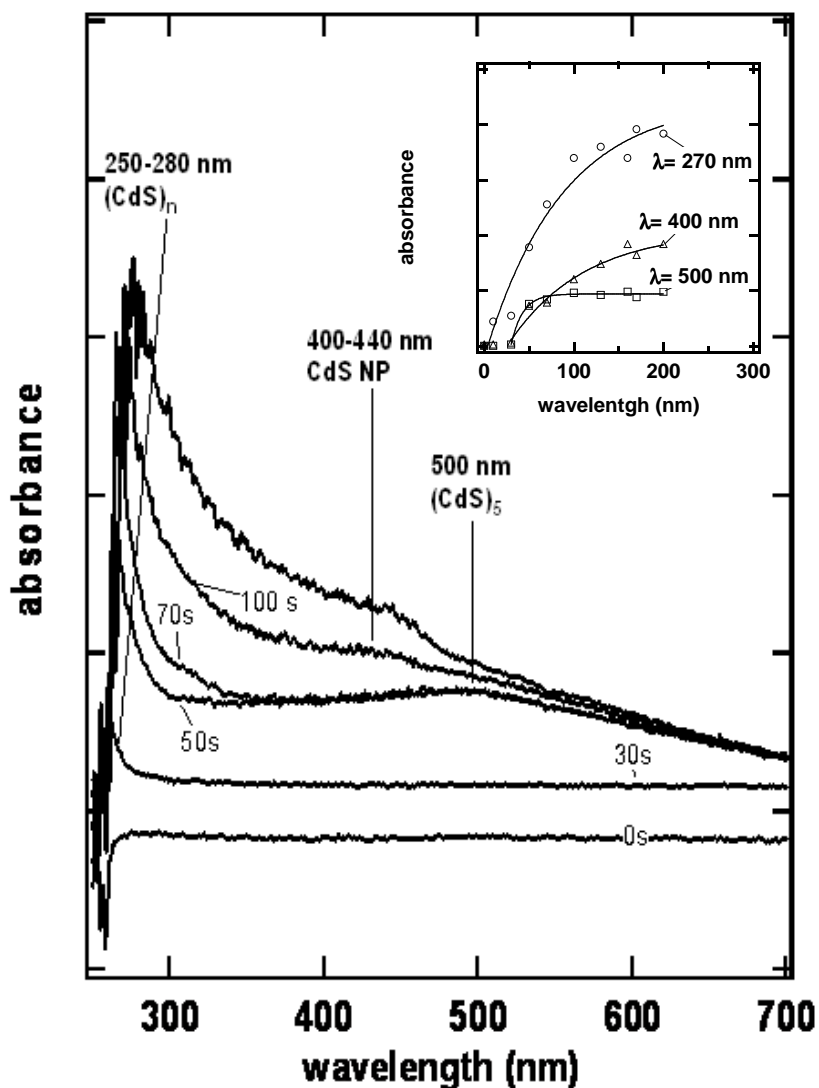


Figure 5.4: The absorption spectra of a diluted  $\text{Cd}(\text{CH}_3\text{CO}_2)_2$  in DMSO solution as a function of microwave exposure time. The insert illustrates the dependence of the absorption at 270, 400 and 500 nm on time.

### 5.6 Theoretical calculations on $(\text{CdS})_n$ and $(\text{Cd}_n\text{S}_{n+1})^{-2}$ clusters.

Why are clusters formed in the microwave assisted synthesis of CdS NP so stable? Joswig, Springborg, and Seifert have reported a decrease in the energy of  $(\text{CdS})_n$  clusters with increasing the number of CdS pairs from 5 to 10. The size of the clusters claimed to form in this work has between 1 and 5 CdS units. We performed theoretical calculations on small CdS clusters,  $n=1$  to

n=4, with the purpose of identifying a barrier to the formation of (CdS)<sub>n</sub> clusters. The optimized structures of the clusters considered are illustrated in figure 5.5. The closed circles in figure 5.5 represent the dependence of the (CdS)<sub>n</sub> cluster energy, obtained at the DFT/B3LYP/DGDZVP level of theory on aggregation number. The total energy is found to decrease linearly, at a rate of about 5800 hartrees/n, with (CdS)<sub>n</sub> aggregation number. The feasibility to form the (CdS)<sub>n</sub> cluster through stepwise polymerization of the CdS may be discussed from consideration of the energy ( $\Delta E$ ) of the reaction between the (CdS)<sub>n-1</sub> cluster and the CdS:



and

$$\Delta E = E(\text{CdS})_n - E(\text{CdS})_{n-1} - E(\text{CdS}) \quad \text{equation 5.1}$$

Values of  $\Delta E$  as a function of CdS aggregation number are indicated by the open circles in the lower graph of figure 5.5. The open squares in the insert represent the dependence of the cluster binding energy,  $E_B$ , on aggregation number, defined as:

$$E_B = -E_n/n + E_1 \quad \text{equation 5.2}$$

We included the value of the energy associated with the formation of CdS monomers from the reaction of Cd<sup>2+</sup> with S<sup>2-</sup>. Reaction 5.1 is found to release energy for all values of n, although the magnitude is sensitive to specific clusters. Cluster stability, on the other hand, increases with  $E_B$ . The dependence of  $E_B$  summarized on figure 5.5 indicates that there is a barrier to form the (CdS)<sub>4</sub> cluster from the reaction between (CdS)<sub>3</sub> and the CdS monomer. The cluster binding energy increases with aggregation number up to n=3 and then decreases for n=4. Thus (CdS)<sub>n</sub>

clusters with aggregation number  $n=1, 2$  and  $3$  are likely to be the dominant species in solution at the early stages of reaction considered here. The most intense band in the spectra of samples exposed to microwave radiation between  $30$  and  $70$  seconds is between  $260$  and  $265$  nm, which has been attributed to absorption of light by the  $(\text{CdS})_2$  cluster.<sup>21</sup>

Since a barrier is present to form the cluster made up of  $4$  monomers, it is important to consider alternative reactions that could lead to the formation of nanoparticles. The  $(\text{CdS})_4$  tetramer could be formed by coupling two dimers. Indeed, coupling two dimers is a process predicted to have a  $\Delta E$  about  $98$  kJ/mol lower than the addition of a monomer to the  $(\text{CdS})_3$  trimer. However, in diluted solutions, other reactions will likely take place due to the limited supply of the cadmium ions. It is likely that small clusters may catalyze the formation of small particles by reacting with the DMSO while heating in the microwave to form  $(\text{Cd}_n\text{S}_{n+1})^{2-}$ :



To test this hypothesis, we performed calculations on a series of  $(\text{Cd}_n\text{S}_{n+1})^{2-}$  clusters, where  $n=1,2$  and  $3$  at the DFT/B3LYP/DGDZVP level of theory. The results on the total energy are indicated by the red circles on figure 5.5. The total energy of the  $(\text{Cd}_n\text{S}_{n+1})^{2-}$  clusters decreases with aggregation number. The energy change associated with reaction 3 increases slightly from  $n=1$  to  $n=2$  and then decreases from  $n=2$  to  $n=3$ . Therefore, formation of non stoichiometry cadmium sulfides from the reactions of  $(\text{CdS})_n$  and DMSO while heating diluted solutions of  $\text{Cd}(\text{CH}_3\text{CO}_2)_2$  in DMSO in the microwave oven remains an open possibility to account for the reactions leading to the formation of larger particles. We extended our calculations to establish the HOMO-LUMO gap in the  $(\text{CdS})_n$  and  $(\text{CdS})_n\text{S}^{2-}$  clusters. We found that the energy gap

between the HOMO and LUMO of these clusters is lower in the ionic clusters than in the  $(\text{CdS})_n$  cluster from which they are derived. Configuration interaction singlet calculations on the structures of CdS monomer and  $\text{CdS}^{2-}$  cluster, optimized at the DFT/DGDZVP level of theory, were performed to gain insight into the optical transitions that are expected. The calculations predict the strongest transitions in the CdS monomer and  $\text{CdS}^{2-}$  cluster ion to occur around 351 and 327 nm, respectively. We note that a tail between 300 and 350 nm is clearly observed in the spectrum that corresponds to the UV-visible absorption measurement when the solution was heated for 70 seconds. We propose the tail to involve transitions of non stoichiometric  $\text{Cd}_n\text{S}_n^{2-}$  clusters based on the predicted transitions of the  $\text{CdS}_2^{2-}$  cluster indicated on table 5.1. This is not unusual. Cheng and coworkers, for instance, found that chloride anions have a major effect on the optical and physical properties of lead hydroxide ( $\text{Pb}(\text{OH})_2$ ) nanostructures. In their work, the above authors established that the optical properties of  $\text{Pb}(\text{OH})_2$  were a sensitive function of the initial chloride ion concentration. Furthermore, they established that a large amount of chloride restrains the formation of  $\text{Pb}(\text{OH})_2$ . Thus changes in the optical absorption spectrum of solutions due to the formation of non stoichiometric cadmium sulfides are a likely to take place in the case presented here, particularly when the  $\text{Cd}^{2+}$  ions are in limited supply.

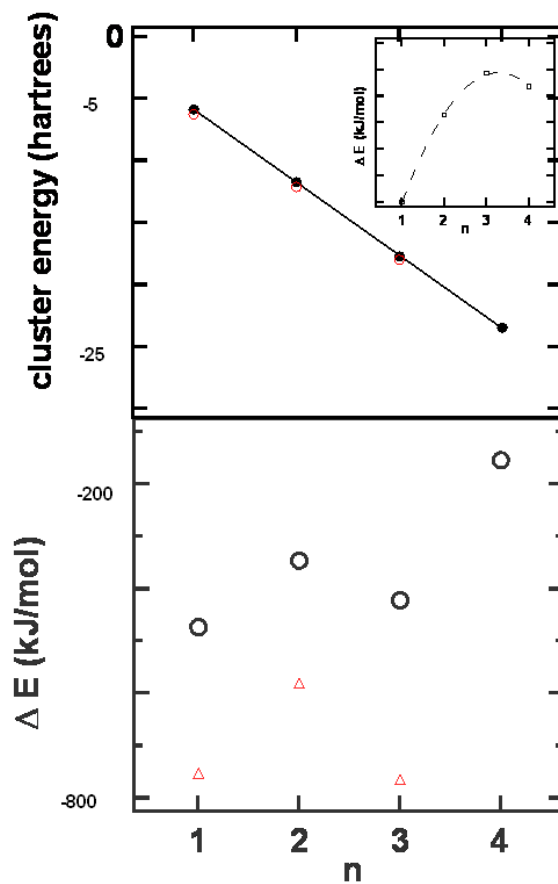


Figure 5.5: The variation of the  $(\text{CdS})_n$  cluster energy on aggregation number  $n$  is indicated by the closed circles in the upper graph of the figure. The energy change associated with the formation of the  $n^{\text{th}}$   $(\text{CdS})_n$  cluster from the  $(n-1)$  cluster and monomer is represented by the open circles in the figure at the bottom of the page. The insert represent the cluster binding energy. The red circles and triangles represent the total energy of the  $(\text{Cd}_n\text{S}_{n+1})^{-2}$  cluster and the energy change from the reaction between  $(\text{CdS})_n$  and  $\text{S}^{2-}$  ion as a function of aggregation number, respectively.

Cluster	Band Gap (eV)	Transition Energy (nm)	Oscillator Strength
CdS	1.5	351.47	0.6
(CdS) <sub>2</sub>	2.31		
(CdS) <sub>3</sub>	3.69		
(CdS) <sub>4</sub>	3.29		
(CdS) <sub>1</sub> S <sup>2-</sup>	0.44	327.67	1
(CdS) <sub>2</sub> S	1.36		
(CdS) <sub>3</sub> S	3.04		

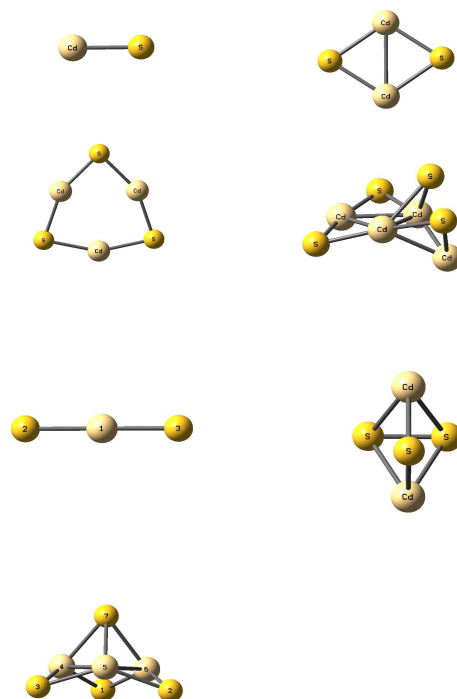
Table 5.1: Band gaps (eV) of Cd<sub>n</sub>S<sub>n</sub> and Cd<sub>n</sub>S<sub>n+1</sub> clusters considered in this work. The transition energies and oscillator strengths corresponding to the strongest transition of the CdS and CdS<sub>2</sub><sup>2-</sup> are also indicated in the table.

### 5.7 CdS Nucleation and Growth.

We also investigated the effect of initial Cd<sup>2+</sup> ion concentration in the nucleation and growth of CdS NP. UV-visible absorption spectra of a 0.001 mg/mL solution of Cd(CH<sub>3</sub>CO<sub>2</sub>)<sub>2</sub> in DMSO as a function of time in a microwave oven are displayed on figure 5.6. The measurements were performed with a high acquisition time to obtain adequate information related to the absorbance at 400 nm and the onset of light absorption at the expense of losing information related to light absorption below 300 nm. The UV visible absorption spectra obtained at times shorter than 30 seconds did not exhibit any signal between 400 and 600 nm above the noise level of the measurements. A small amount of light absorption in the visible region of the spectrum can be identified in the measurements obtained after the solution is placed in the microwave oven for 80 seconds. The species that gave rise to the absorption band around 500 nm in the diluted solutions discussed in the previous section is no longer observed in the more concentrated

solutions. Well defined absorption spectra are obtained when the solutions are exposed to microwave radiation for period of times longer than 90 seconds. The spectrum of solutions exposed to microwave radiation for this period of time exhibits an onset of light absorption around 470 nm and an increase in absorption that extends to shorter wavelengths. Adding about 1 mL of ethanol to a 0.003 mg/mL  $\text{Cd}(\text{CH}_3\text{CO}_2)_2$  in DMSO solution exposed to microwave radiation for 150 s resulted in the spectrum displayed in the inset of figure 5.6. The spectrum is dominated by bands around 260 nm and 320 nm and a weaker band due to CdS NP absorption around 400 nm.

Scheme 5.2: The optimized structures of  $(\text{CdS})_n$  and  $(\text{Cd}_n\text{S}_{n+1})^{-2}$  clusters investigated theoretically in this work.



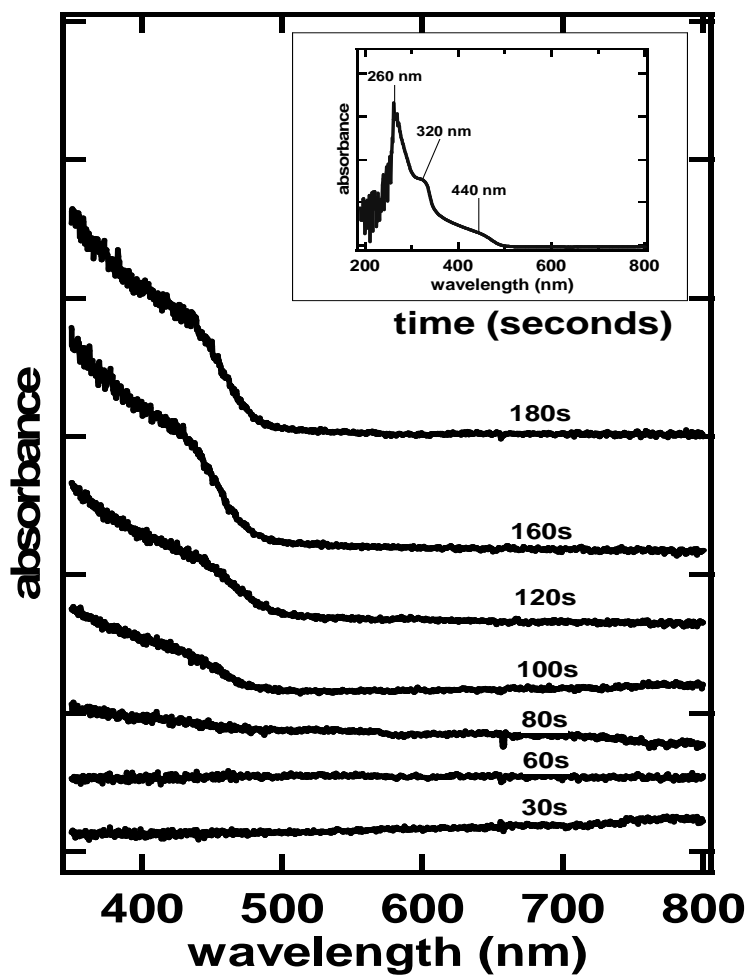


Figure 5.6: Absorption spectra of a 0.001 mg/mL Cd(CH<sub>3</sub>CO<sub>2</sub>)<sub>2</sub> in DMSO solution as a function of time in the microwave. A typical absorption spectrum of the solution after exposure to microwave radiation for 150 seconds and further diluted with 1 mL of ethanol is illustrated in the inset.

### 5.7.1 CdS Nucleation

The absorbance is related to the number of nuclei formed according to Beer-Lambert's law:

$$A = \alpha \ell [N] \quad \text{equation 5.3}$$

where  $\alpha$  represent the absorptivity coefficient,  $\ell$  is the optical length and  $[N]$  represent the concentration of absorbers. Since CdS nanoparticles are a semiconductor, it is convenient to use the absorbance near the band edge to establish the number of absorbers in solution. The dependence of the absorbance at 400 nm on heating time for initial  $[\text{Cd}(\text{CH}_3\text{CO}_2)_2]_0$  concentrations of 0.0005, 0.001 and 0.003 g/mL is illustrated in figure 5.7. The measurements were performed with a high acquisition time to obtain information related to the absorbance at 400 nm and the onset of light absorption. The absorbance at 400 nm is below the detection levels of our instrument in samples exposed to microwave heating for 30 seconds or less and initial  $[\text{Cd}(\text{CH}_3\text{CO}_2)_2]_0$  smaller than 0.001 g/mL while it is found slightly above the noise level in samples with  $[\text{Cd}(\text{CH}_3\text{CO}_2)_2]_0 = 0.003$  mg/mL. The absorbance of solutions with  $[\text{Cd}(\text{CH}_3\text{CO}_2)_2]_0$  of 0.001 and 0.003 mg/mL at 400 nm is independent of initial reactant concentration up to about 200 seconds. This result leads us to conclude that the formation of nuclei is independent of the supply of  $\text{Cd}^{2+}$  for this initial  $[\text{Cd}(\text{CH}_3\text{CO}_2)_2]_0$  concentrations. Since nuclei formation requires the formation of CdS clusters, we conclude that the nucleation process for initial  $[\text{Cd}(\text{CH}_3\text{CO}_2)_2]_0$  concentrations larger than 0.001 mg/mL is limited by the supply of sulfide ions.

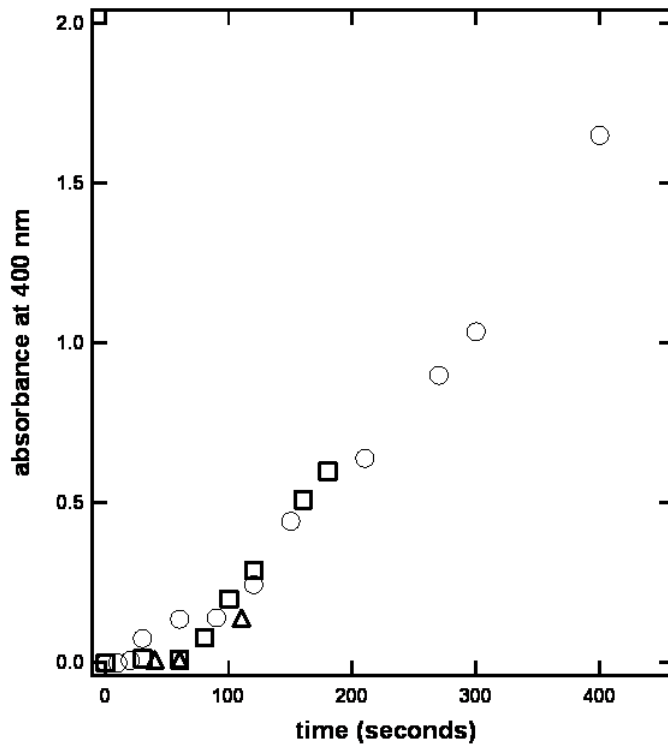


Figure 5.7: The dependence of the absorbance at 400 nm on time for solutions with  $[\text{Cd}(\text{CH}_3\text{CO}_2)_2]_0$  of 0.0005 (triangles), 0.001 (squares) and 0.003 (circles) mg/mL.

### 5.7.2 Growth of CdS NP

The band gap in NP that exhibit quantum confinement effects is related to nanoparticle radius (R) according to:

$$E_g(\text{NP}) = E_g(\text{bulk}) + \left( \frac{\hbar^2}{8R^2} \right) \left( \frac{1}{m_e} + \frac{1}{m_h} \right) - \frac{1.8e^2}{4 \epsilon_0 \epsilon R} \quad \text{equation 5.4}$$

where  $E_g(\text{NP})$  and  $E_g(\text{bulk})$  represent the band gap of the NP and bulk semiconductors, respectively. The electron and hole masses are represented by  $m_e$  and  $m_h$ , respectively, in equation 5.4. The second term of the above equation is the quantum energy of localization, and the third term represents the energy of Coulomb attraction.<sup>22</sup> Caponetti and coworkers<sup>22</sup> found

that CdS NP diameter ( $d$ ) and the wavelength that corresponds to the onset of light absorption ( $\lambda$ ) can be quantitatively modeled with the power law:

$$\lambda = k d^n \quad \text{equation 5.5}$$

where  $d$  and  $k$  represent the particle diameter and growth constant and  $n$  is a power exponent. Based on equation 5.5 we estimate that particles with an onset of light absorption between 450 and 500 nm are expected to have diameters in the 40 to 50 nm range.

CdS is a direct semiconductor. Accordingly, the wavelength that corresponds to the point at which the absorbance has fallen to zero corresponds to the onset of light absorption. The insert in figure 5.8 shows a plot of the product of  $(A/\lambda)$  as a function of  $1/\lambda$  for a solution of the CdS NP prepared in DMSO and further dispersed in 1 mL of ethanol. Since the absorbance is proportional to the product of  $(A/\lambda)^2$ , the point at which  $(A/\lambda)^2$  is equal to zero is taken as the onset of light absorption. For the sample examined in the inset, we estimate the onset of light absorption around 480 nm from the plot of  $(A/\lambda)^2$  as a function of  $1/\lambda$ . We notice that the approach provides information related to the largest particles in solution as oppose to the mean or average particle size in solution.

We have used the approach described in the previous paragraph to estimate the onset of light absorption as a function of microwave exposure time. The open squares and circles in figure 5.8 represent the onset of light absorption as a function of heating time for solutions with initial  $[\text{Cd}(\text{CH}_3\text{CO}_2)_2]_0$  of 0.001 and 0.003 mg/mL. The increase in the onset of light absorption with time between 100 and 180 seconds appears to be independent of initial  $\text{Cd}(\text{CH}_3\text{CO}_2)_2$  concentration, despite the fact that the two concentrations compared are in a ratio of 3:1. This

indicates that the growth is not limited by the amount of  $\text{Cd}^{2+}$  present in this initial  $[\text{Cd}(\text{CH}_3\text{CO}_2)_2]_0$  concentration range.

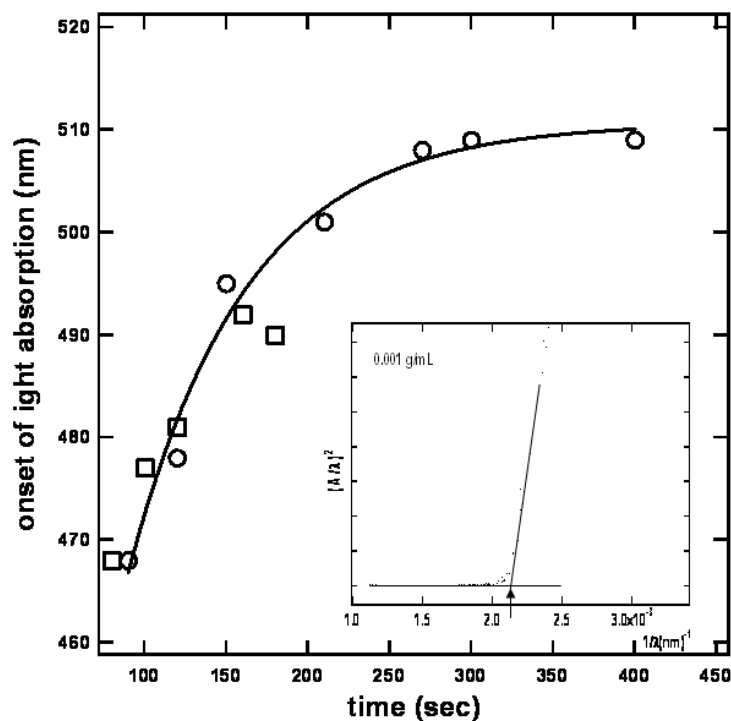


Figure 5.8: The open rectangles and circles represent the onset of light absorption as a function of heating time of 0.001 and 0.003 mg/ mL  $\text{Cd}(\text{CH}_3\text{CO}_2)_2$  in DMSO solutions, respectively. A representative plot of  $(A/\lambda)^2$  as a function of  $(1/\lambda)$  used to estimate the onsets of light absorption is illustrate in the insert.

In samples heated in the microwave oven for times shorter than 200 seconds, the onset of light absorption is observed at wavelengths that are between 44 and 10 nm lower than the one observed in bulk CdS. This result is consistent with quantum confinement effects in the CdS nanoparticles formed upon exposure of the solution to microwave radiation for period of times shorter than  $\sim 200$  seconds. The onset of light absorption increases slightly with further increase in microwave irradiation time. It is set around 510 nm in samples exposed to microwave radiation for periods of time between 300 and 400 seconds. This value is, within the

experimental uncertainty of our measurements, close to the band gap observed in bulk CdS. This observation lead us to conclude that CdS particles formed after 200 seconds of microwave radiation do not exhibit quantum confinement effects.

Two independent experiments were performed to establish that heating is required for the nucleation and growth process. In the first one, a solution containing the CdS NP, prepared by exposing the  $\text{Cd}(\text{CH}_3\text{CO}_2)_2$  in DMSO solution to microwave radiation for 180 seconds, was allowed to age over a prolonged period of time. Absorption spectra of dispersions prepared by exposing the solution to microwave radiation for about 180 seconds measured one day and up to two months after their preparation are illustrated on figure 5.9. The absorption spectra displayed on figure 5.9 overlap with each other, regardless of the aging time of the sample. We conclude that there is no nucleation or growth in the absence of heating. In a second experiment, the sample was heated in the microwave for a longer period of time, in the neighborhood of 500 seconds. A representative FESEM image of a deposit prepared from the resulting CdS particles is displayed in the lower half of figure 5.9. The image reveals CdS particles as large as 250 nm as well as agglomerates of smaller CdS particles, some of which are about 25 nm in diameter. The observation of large particles in the FESEM measurements upon further heating the sample indicates, combined with the absence of nucleation and growth upon aging at room temperature, that there is a barrier to nanoparticle formation. Also, EDAX mapping for Cadmium and Sulfur atoms was performed in order to establish the purity of the sample. Figure 5.10 show the EDAX mapping obtained for the FESEM of 180s sample.

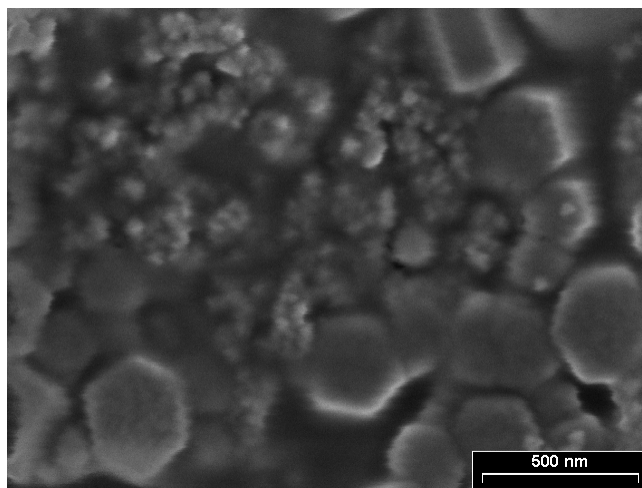
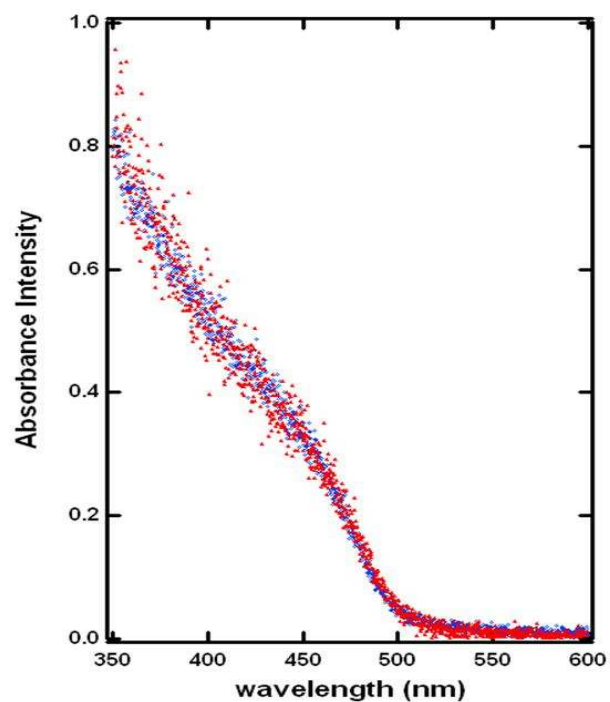


Figure 5.9: The solid and dotted spectra illustrate the absorption spectra of the CdS NP prepared immediately and two months after their preparation, respectively. FESEM images of a CdS NP solution prepared from exposing the  $\text{Cd}(\text{CH}_3\text{CO}_2)_2$  in DMSO solution to microwave radiation for over 300 seconds.

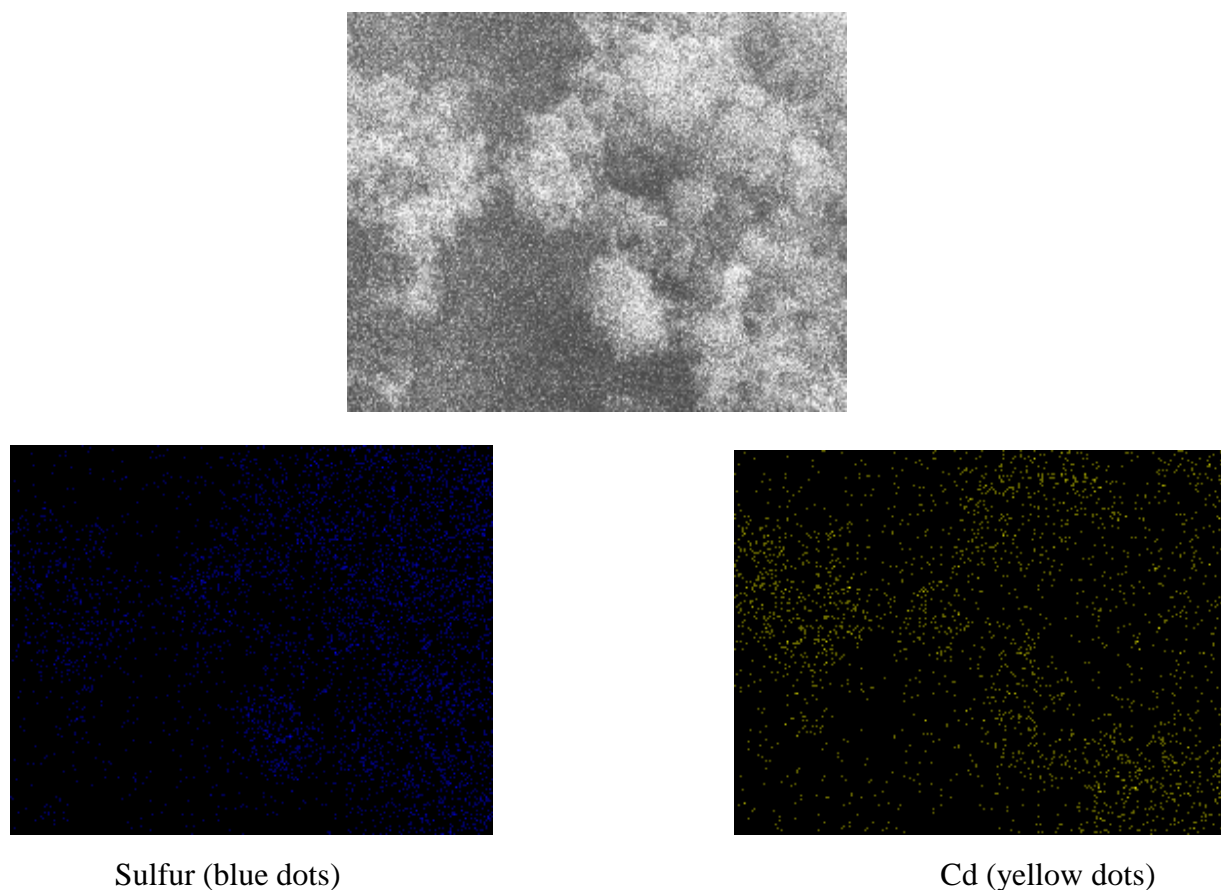


Figure 5.10: EDAX mapping for FESEM image. EDAX mapping was used for the identification of Cd and Sulfur atoms.

## 5.8 Discussion

Microwave heating is an attractive approach to the synthesis of CdS NP from the reactions of Cd(CH<sub>3</sub>CO<sub>2</sub>) in DMSO. The use of a single precursor to supply the sulfide ions combined with the fast and local heating conditions employed to initiate the reactions that results in CdS NP presents a unique advantage to observe spectroscopic signatures that may be associated to embryos and clusters that lead to the formation of nuclei or particles. In the context of classic nucleation theory, an embryo may be regarded as an unstable nucleus which may split into its precursors or become stable nuclei if enough energy ( $\Delta G^*$ ) is supplied to overcome a barrier to reach a critical size,  $r^*$ :

$$\Delta G^* = 16\pi\gamma^3 / (3 |\Delta\mu|^2) \quad \text{equation 5.6}$$

where  $\gamma$  and  $\Delta\mu$  represent the surface tension and the difference in energy between the embryos and nuclei phases.

In the process of making nuclei, embryos may be involved in different reaction pathways, each having a barrier. According to equation 5.6, these barriers may be discussed in the context of the thermodynamic feasibility to make a given clusters. In this regard, the DFT calculations discussed earlier are a useful tool to guide a discussion. The calculations indicate that all the embryos considered here have a lower energy than the corresponding parent ions. Thus successive addition of monomers to embryos will likely proceed continuously until a barrier is reached. This critical barrier sets the diameter and size of the cluster. Taking into account thermodynamic arguments alone, as dictated by equation 5.6, the calculations summarized in the lower panel of figure 5.5 indicate that there is a barrier to form the  $(\text{CdS})_4$  thru the stepwise polymerization of the monomer. The presence of this barrier allows for alternative reaction pathways, like the formation of a different family of clusters,  $(\text{Cd}_n\text{S}_{n+1})^{2-}$ . These clusters are more stable than the  $(\text{CdS})_n$  cluster they are derived from. Furthermore, the amount of energy released to form sulfides from the reactions of  $(\text{CdS})_n$  and  $\text{S}^{2-}$  is larger than the energy required to form the corresponding  $(\text{CdS})_n$  cluster they are derived from. Turning “on” the microwave allows  $(\text{CdS})_n$  and  $(\text{Cd}_n\text{S}_{n+1})^{2-}$  cluster to further react to form nuclei. Turning “off” the microwave shuts down the supply of energy to overcome energy barriers that result in the formation of larger embryos and nuclei.

The TEM measurements are performed on a dry deposit of a 0.001 mg/mL solution heated in the microwave for about 150 seconds and further diluted in ethanol. The dependence of the

absorbance on time displayed on figure 6 shows that for  $t = 150$  seconds a few nuclei are formed. The TEM measurements helps to set an upper limit of  $(1.6 \pm 0.3)$  nm on the size of stable nuclei formed in the process. The absorption spectrum of nanocrystalline CdS NP measuring about 1.9 nm has been recently reported by Li and coworkers.<sup>23</sup> The absorption spectrum of 1.9 nm CdS NP exhibit a single band centered at 375 nm: bands at 322, 351 and 378 nm are observed in the time profile of the synthesis of the nanoparticles and have been attributed to a different CdS species coexisting during the different stages of the synthesis. The spectrum displayed in the insert of figure 5.6 corresponds to the same sample examined in the TEM, which required further dilution with ethanol. We note that the spectrum is dominated by bands at 260, 320 and 440 nm. In the context of the discussion presented in the previous paragraphs, the bands at 260 and 320 nm result from light absorption by clusters while the band at 440 nm results from light absorption by CdS NP. It is important to highlight that the arguments presented in this discussion emerge from stationary measurements. It will be of great importance to perform spectroscopic, as well as temperature, measurements on the synthesis process in situ and inside the microwave oven, to establish the chemical intermediates under the actual reaction conditions.

## 5.9 Conclusion

The synthesis of CdS clusters and nanoparticles from the reaction between  $\text{Cd}^{2+}$  and DMSO in a microwave oven has been studied with UV-visible absorption spectroscopy and transmission electron microscopy. DMSO serves as the solvent and a controlled source of sulfide ions to form  $(\text{CdS})_{1 < n < 5}$  clusters at the early stages of the process. DFT calculations establishes a barrier to the formation of  $(\text{CdS})_4$ . Formation of  $(\text{Cd}_n\text{S}_{n+1})^{2-}$  is proposed in diluted solutions. The clusters grow into CdS nanoparticles, with diameters that range, depending on initial concentration and heating time, from 1.6 nm up to over 250 nm. The time dependence of the onset of light

absorption and absorbance are consistent with a concurrent nucleation and growth processes. The formation of the clusters and nuclei as well as the growth of CdS NP is controlled by turning “on” and “off” the energy supply consistent with an energy barrier to CdS nanostructures formation.

### 5.10 Acknowledgement

EF acknowledges a PhD scholarship from the Sloan Foundation and a scholarship from the Puerto Rico Infrastructure Development Company (PRIDCo). FZ and SN acknowledge undergraduate student support from the UPRM Biominds Program. MG acknowledges financial support from a PhD scholarship from the Sloan Foundation. Partial financial support from the UPRM Department of Chemistry is gratefully acknowledged. EF thanks Hewlett Packard for an internship at the HP PR facilities.

### 5.11 References

1. R Bhattacharya, S.Saha.; Growth of CdS nanoparticles by chemical method and its characterization. *Journal of Physics* **2008**: 71(1) 187-192.
2. Jun Zhang, Lingdong Sun, Chunsheng Liao, Chunhua Yan.; Size Control and photoluminescence enhancement of CdS nanoparticles prepared via reverse micelle method. *Solid State Communication* **2002**: 124 45-48.
3. Tiziana Di Luccio, Anna Maria Laera, Leander Tapfer, Susanne Kempter, Robert Kraus, Bert Nickel.; Controlled Nucleation and Growth of CdS Nanoparticles in a Polymer Matrix. *J.Phys.Chem.B* **2006**: 110 12603-12609.
4. Diaz, David, Mario Rivera, Tong Ni, Juan Carlos Rodriguez, Silvia-Elena Castillo-Blum, Dattatri Nagesha, Juvencio Robles, Octavio-Jaime Alvarez-Fregoso, and Nicholas A. Kotov.; Conformation of Ethylhexanoate Stabilizer on the Surface of CdS Nanoparticles. *J.Phys. Chem B* **1999**: 103 9854-9858.

5. V.P. Singh, R.S. Singh, G.W. Thompson, V. Jayaraman, S. Sanagapalli, V.K. Rangari. Characteristics of nanocrystalline CdS films fabricated by sonochemical methods for solar cell applications. *Solar Energy Materials and Solar Cells* **2004**: 81 293-303.
6. Manoj E. Wankhede, Santosh K. Haram.; Synthesis and Characterization of Cd- DMSO Complex Capped CdS Nanoparticles. *Chem.Mater* **2003**: 15 1296-1301.
7. N. Revaprasadu, S.N. Mlondo.; Use of metal complexes to synthesize semiconductor nanoparticles. *Pure Appl.Chem.* **2006**: 78(9) 1691-1702.
8. P.K. Khanna and Narendra Singh.; Light emitting CdS quantum dots in PMMA: Synthesis and optical studies. *J. of Luminescence* **2007**: 127 474-482.
9. U. Resh, A. Eychmuller, M. Haase and H. Weller. ; Absorption of Fluorescence Behavior of Redispersible CdS Colloids in Various Organic Solvents. *Langmuir* **1992**: 8 2215-2218.
10. Nima Taghavinia, Azam Iraj-zad, S. Mohammad Mahdavi and M. Reza-esmaili. ; Photo-induced CdS nanoparticles growth. *Physica E* **2005**: 30 114-119.
11. Kenneth S. Suslick. ; Sonochemistry. *Science* (1990): 247 (4949) 1439-1445.
12. Liang Li, Huifeng Qian and Jicun Ren.,; Rapid synthesis of highly luminescent CdTe nanocrystals in the aqueous phase by microwave irradiation with controllable temperature. *Chem. Commun.*, **2005**, 528–530
13. S. Martinez, T. Serrano, I. Gomez, A. Hernandez.; Synthesis and Characterization of CdS nanoparticles by microwave irradiation. *Bol.Soc.Esp.Ceram.* **2007**: 46(2) 97-101.
14. Junjie Zhu, Miaogao Zhou, Jinzhong Xu and Xuehong Liao.; Preparation of CdS and ZnS nanoparticles using microwave irradiation. *Materials Letters* **2001**: 47, 25-29.
15. Privman, V. Diffusional Nucleation of Nanocrystals and Their Self-Assembly into Uniform Colloids. *J. Optoelectronics Adv. Mater.* **2008**, 10, 2827-2839.
16. Wang, C. X.; Yang, G. W. Thermodynamics of Metastable Phase Nucleation at the Nanoscale. *Mat. Sci. Eng. R* **2005**: 49, 157-202.
17. Tobler, D. J.; Shaw, S.; Benning, L. G. Quantification of Initial Steps of Nucleation and Growth of Silica Nanoparticles: An *in-situ* SAXS and DLS Study. *Geochim. Cosmochim. Ac.* **2009**, 73, 5377-5393.

18. Abe'cassis, B.; Testard, F.; Spalla, O.; Barboux, P. Probing In Situ the Nucleation and Growth of Gold Nanoparticles by Small-Angle X-ray Scattering. *Nano Lett.* **2007**: 7, 1723-1727.
19. Rivka Elbaum, Shimon Vega, Gary Hodes.; Preparation and Surface Structure of Nanocrystalline Cadmium Sulfide Precipitated from Dimethyl Sulfoxide Solutions. *Chem.Mater* **2001**: 13 2272-2280.
20. Roman Gajda, Andrzej Katrusiak.; Electrostatic Matching versus Close-Packing Molecular Arrangement in Compressed Dimethyl Sulfoxide (DMSO) Polymorphs. *J.Phys.Chem.B* **2009**: 113 2436-2442.
21. Hongxia Zeng, Raji Reddy Vanga, Dennis S. Marynick, and Zoltan A. Schelly, "Cluster Precursors of Uncapped CdS Quantum Dots via Electroporation of Synthetic Liposome. Experiments and Theory" *J. Phys. Chem. B* **2008**: 112, 14422–14426.
22. E. Caponetti, L. Pedone, D. Chillura Martino, V. Panto , V. Turco Liveri. ; Synthesis, size control, and passivation of CdS nanoparticles in water/AOT/n-heptane microemulsions. *Materials Science and Engineering C* **2003**: 23 531–539.
23. Minjie Li, Jianying Ouyang, Christopher I. Ratcliffe, Laetitia Pietri, Xiaohua Wu, Donald M. Leek, Igor Moudrakovski, Quan Lin, Bai Yang, and Kui Yu, ACS Nano, CdS Magic-Sized Nanocrystals Exhibiting Bright Band Gap Photoemission via Thermodynamically Driven Formation **2009**: 3(12), p.3832 – 3838.
24. Ferrer Torres, Edmy J., Rivera D., Gonzalez, Miguel and Miguel E. Castro. Turning "ON"and "OFF" nucleation and growth: microwave assisted síntesis of CdS Clusters and nanoparticles. Accepted in December 2010 in *Materials Research Bulletin*.

### Additional References

- C. Unni, Daizy Philip, S.L. Smitha, K.M. Nissamudeen, K.G. Gopchandran.; Aqueous synthesis and characterization of CdS, CdS:Zn<sup>2+</sup> and CdS:Cu<sup>2+</sup> quantum dots. *Spectrochimica Acta Part A:Molecular and Biomolecular Spectroscopy* **2009**: 72(4) 827-832.
- W.Ronald Fawcett, Alla A. Kloss.; Solvent-Induced Frequency Shifts in the Infrared Spectrum of Dimethyl Sulfoxide in Organic Solvents. *J.Phys.Chem.* **1996**: 100 2019-20-24.

- Yanhong Zhang, Yongming Chen, Haijun Niu, Mingyuan Gao.; Formation of CdS Nanoparticle Necklaces with functionalized Dendronized Polymers. *Small* **2006**: 11 1314-1319.
- Roman Gajda, Andrzej Katrusiak.; Electrostatic Matching versus Close-Packing Molecular Arrangement in Compressed Dimethyl Sulfoxide (DMSO) Polymorphs. *J.Phys.Chem.B* **2009**: 113 2436-2442.
- Thelma Serrano, Idalia Gomez, Rafael Colas, Jose Cavazos.; Synthesis of CdS nanocrystals stabilized with sodium citrate. *Eng.Aspects* **2009**: 338 20-24.
- G.Z. Wang, W.Chen, C.H. Liang, Y.W.Wang, G.W. Meng and L.D. Zhang.; Preparation and characterization of CdS Nanoparticles by ultrasonic radiation. *Inorganic Chemistry Communications* **2001**: 4(1) 208-210.
- Qiyu Yu and Chun-Yan Liu.; Study of Magic Size –Cluster Mediated formation of CdS Nanocrystals: Properties of the Magic-Size Clusters and Mechanism Implications. *J. Phys. Chem.* **2009**: 113 12766-12771.
- X. Y. Liu, *J. Phys. Chem. B* **2001**: 105, 11550-11558
- Cheng Jin, Zou Xiao-Ping, Song Wei-Li, Cao Mao-Sheng, Su, Yang Gang-Qiang, Lu Xue-Ming, Z Fu-Xue, Zhang.; Shape-Controlled Synthesis and Related Growth Mechanism of Pb(OH)<sub>2</sub> Nanorods by Solution-Phase Reaction. *CHIN. PHYS. LETT.* **2010** 27 (5); 057302-1 to 057302-4.
- Jin Cheng, Xiaoping Zou, Weili Song, Xiangmin Meng, Yi Su, Gangqiang Yang, Xueming Lü, Fuxue Zhang and Maosheng Cao.; Effects of concentration of chloride anion on the morphology and microstructure of precipitates from lead nitrate solutions. *CrystEngComm*, **2010**, 12, 1790-1794.
- Xiao-Ling Shi, Mao-Sheng Cao, Jie Yuan, Quan-Liang Zhao, Yu-Qing Kang, Xiao-Yong Fang, and Yu-Jin Chen.; Nonlinear resonant and high dielectric loss behavior of CdS/ $\alpha$ -Fe<sub>2</sub>O<sub>3</sub> heterostructure nanocomposites. *Appl. Phys. Lett.* **2008**, 93, 183118.

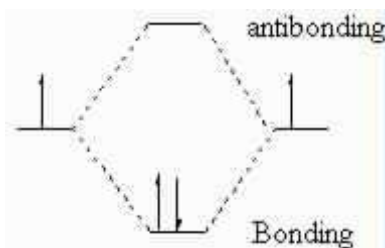
## CHAPTER 6: Fluorescence response of CdS nanoparticles to serum of cardiac patients: towards the development of a real time sensor for heart failure detection.<sup>34</sup>

---

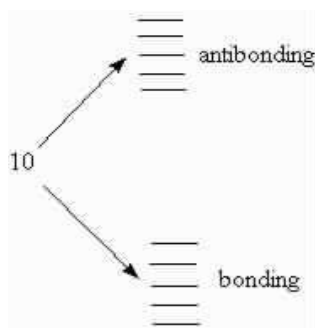
### 6.1 Introduction

#### 6.1.1 Introduction to basic solid state physics concepts

The sensing capabilities of quantum particles are largely limited by their electronic properties. The structure of a solid provides the basis for the description of metals and semiconductors and account for their unique chemical and physical properties. The molecular orbital theory, with which chemists are more acquainted with, is a good aid to understand these properties. These molecular orbitals are described by wave functions and have different energies. According to MO theory, N molecular orbitals are formed from the interaction of N atomic orbitals. For instance, consider a molecule with two atomic orbitals. The result must be that two molecular orbitals will be formed from these atomic orbitals: one bonding and one antibonding, separated by certain energy<sup>1</sup>.

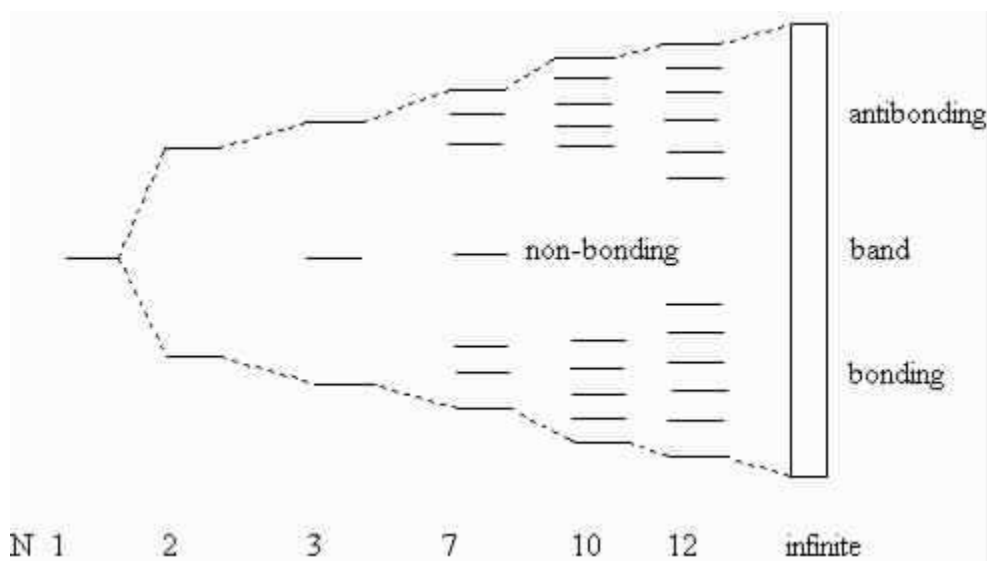


A molecule with ten atoms will produce 10 molecular orbitals: five bonding and five antibonding. If we take a close look at the separation among each set of orbitals, as the number of molecular orbitals increases, the energy difference between the lowest bonding and the highest antibonding orbitals generally increases, while *the space between each individual orbital decreases*.



Prashant V. Kamat. "Photophysical, Photochemical and Photocatalytic aspects of metal nanoparticles". 2002. J.Phys.Chem. B 106; 7729-7744.

Now consider a metal with an infinite number of atoms. This will form an infinite number of molecular orbitals so close together that they blur into one another forming a band. This whole process is shown below.



Prashant V. Kamat. "Photophysical, Photochemical and Photocatalytic aspects of metal nanoparticles". 2002. J.Phys.Chem. B 106; 7729-7744.

In the above image, the origin of the band becomes quite clear because as the number of molecular orbitals increases, the bonding and antibonding orbitals get closer together, filling in the middle. This results in the band shown on the right side of the figure. It becomes quite clear that the molecular orbitals become blurred and hence mix with each other, which gives rise to the

delocalized cloud of electrons that metals are said to possess. By describing the molecular orbitals of certain materials as bands, it becomes much easier to understand the properties of metals and semi-metals.

The electronic distribution of electrons gives rise to three categories: conductors, semiconductors and insulators. In metals, electrons can move freely among the orbitals within an energy band as long as the orbitals in the band are not completely occupied. In semiconductors and insulators, on the other hand, there is a well defined energy gap between the orbitals with the highest and lower energy. The magnitude of the energy gap is traditionally used to distinguish insulators and semiconductors: the larger the gap the material has the more likely it will be considered as an insulator.

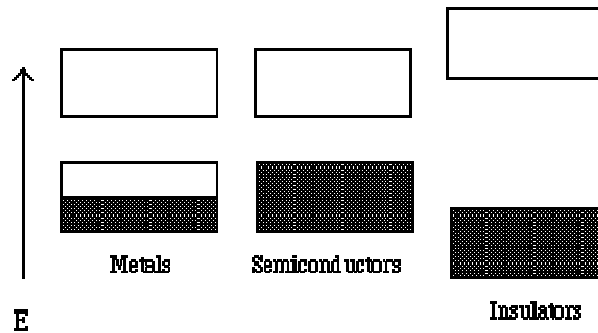


Figure 6.1: The energy bands of metals, semiconductors and insulators. For insulators and semiconductors, the lower band is called the valence band and the higher band is called the conduction band. The lower energy band in metals is partially filled with electrons.

The simplest model for a metal is the free electron model<sup>2</sup>. This model makes ignores interactions among electrons. The Schrodinger equation:

$$(-\hbar^2/2m)\nabla^2\Psi = E\Psi$$

**equation 6.1**

is solved subject to periodic boundary conditions resulting in wavefunctions ( $\Psi(r)$ ) with the general form  $\Psi(r) = N \exp(ik \cdot r)$  and allowed energy states given by  $E = \hbar^2 k^2 / 2m$ . The allowed energy states results in a continuum dependence of E on the propagation constant k. The periodic boundary conditions results in discrete values for  $k=2\pi n/L$ , where L represents de length at which the periodicity is present, and is n is an integer.

Bragg reflection of the electron wave gives rise to bands. At the points where Bragg reflection occurs, wavelike solutions to the Schrodinger equation do not exist. The Bragg condition is:

$$(\bar{G} + \bar{k})^2 = k^2$$

**equation 6.2**

In one dimension the condition becomes:

$$k = \pm(n \cdot \pi) / a$$

**equation 6.3**

where  $n=1,2,3,\dots$  and a is the lattice constant.

The first reflection occurs at  $n=\pm 1$  and the region between  $n= +1$  and  $n= -1$  in a plot of E as a function of k becomes an allowed region, as oppose to a discrete level, with slight variations in E due to the interaction of electrons and ion cores. The second refecton occurs at  $n= \pm 2$ , the third at  $n= \pm 3$  and so on. These regions constitute Brillouin zones and each one of them represent a band. The energy gap  $E_g$  is associated with the first Bragg reflection at the first Brillouin zone boundary and represents the energy difference between the two adjacent bands at  $n=\pm 1$  and  $\pm 2$ .

Qualitatively, the Bragg reflections at the zone boundaries will make standing waves in the crystal. There are two different standing waves that can occur: one representing the difference of a right and a left-directed wave and one representing the sum of a right and a left-directed wave. The Bragg reflection is a characteristic feature of wave propagation in crystals. Bragg reflection of electron waves in crystals is the cause of energy gaps, at Bragg reflection wavelike solutions of the Schrödinger equation do not exist. These energy gaps are determinants for classifying the solid as an insulator or a conductor.

The standing wave 2, piles up electrons around the positive ion cores, which means that the average potential energy will be lower than a free traveling wave (constant probability density). The potential energy corresponding to standing wave 1 will have higher potential energy than a free traveling wave, since it piles up electrons between the ion cores (not compensated by positive ions). The energy difference between the standing waves is the origin to the energy gap  $E_g$ . The relation between the electron energy and the electron wave vector is called the band structure. The band structure is directly related to the crystal structure of the material.

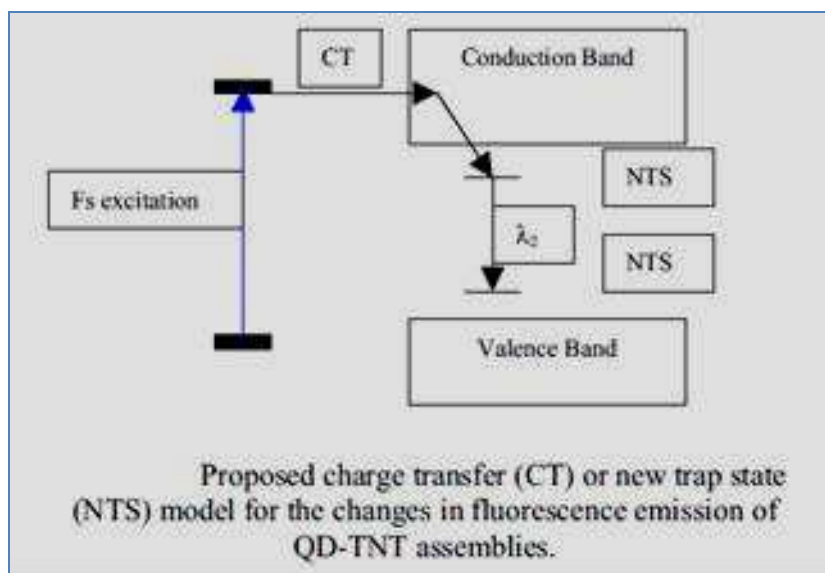
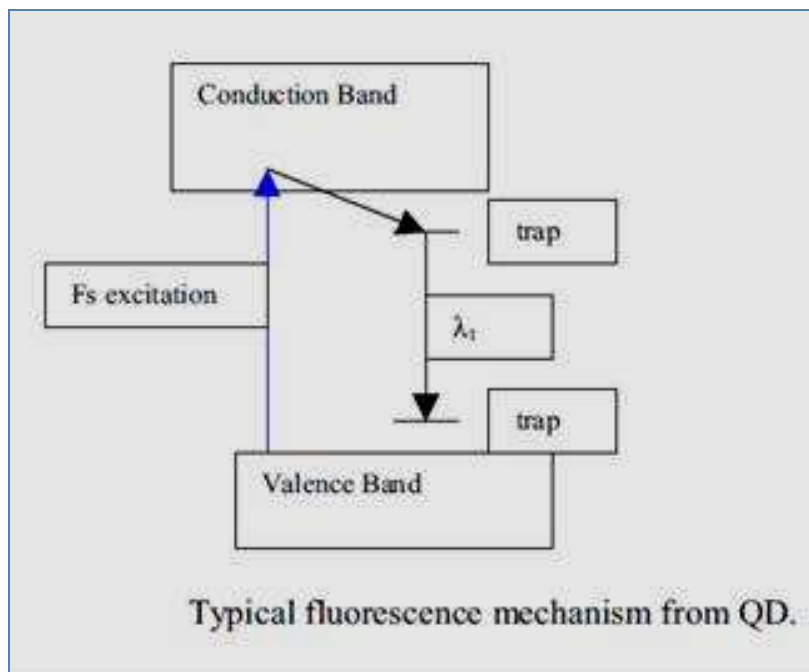
### **6.1.2 Quantum size effects.**

The small size results in new quantum phenomena that yield some extraordinary bonuses. Material properties change dramatically because quantum effects arise from the confinement of electrons and "holes" in the material. Size changes other material properties, such as the electrical and nonlinear optical properties of a material, making them very different from those of the material's bulk form. The quantum size effect is involved when the de Broglie wavelength of the valence electrons is of the same order as the size of the particle itself. Then, the particles

behave electronically as zero dimensional quantum dots or quantum boxes driven by quantum mechanics rules. If a dot is excited, the smaller the dot, the higher the energy and intensity of its emitted light. Hence, these very small, semiconducting quantum dots are gateways to an enormous array of possible applications and new technologies. Gammon, Daniel et. al., made optical studies of single quantum dots<sup>16</sup>. Quantum dots measure between 1-100 nm, are semiconductor structures in which the electron wavefunction is confined in all three dimensions by the potential energy barriers that form quantum dot boundaries. A quantum dot, QD, electronic response, like that of a single atom, is manifest in its discrete energy spectrum, which appears when electron-hole pairs are excited. Although the wavefunction of a QD electron, and its corresponding hole, extends over many thousand lattice atoms, the pair termed an exciton behaves in a quantized and coherent fashion. The coherence is relatively easy to detect and control optically. Another attractive property of the quantum dot is that their size, shape and composition can all be tailored to create a variety of desired properties.

Many types of quantum dots materials have been developed, electrostatic and epitaxial QDs for example. Researchers have made a flurry of new and direct observations of fine structure splittings, hyperfine shifts and so on. These splitting contain the details of spin interactions and other quantum properties. The interaction of energy between excitons leads to the possibility of generating single photons on demand. A strong laser pulse can create a state of many excitons, each of which has a different energy. But only one photon is emitted at the single exciton transition energy. A narrow band pass filter tuned to the single exciton emission line can therefore be used to realize a solid-state source of single photons. One of the goals driving QD research, and nanostructure research is the creation of complex nanomaterials with customized properties.

In practice, however, trap states are always present in semiconductor nanostructures. These states were briefly discussed in the previous chapter. These states are likely to play a central role in the sensing capabilities and future applications of semiconductor nanostructures. S. Nieto et. al. studied nanoscaled sensing for quantum dots fluorescence quenching for nitrated explosives<sup>17</sup>. Nanoscaled semiconductors have the potential to be employed in trace explosive detection. They reported the effect of 2,4,6 trinitrotoluene on the fluorescence emission of zinc sulfide (ZnS) protected cadmium selenide (CdSe) quantum particles. The fluorescence was excited off resonance with respect to the quantum dots, but close to the absorption band edge of the TNT. The results presented were consistent with the extensive quenching and a change in fluorescence emission of QD by TNT. They found that the second wavelength (quantum dots plus TNT) was distinct from the emission wavelength ( $\lambda_1$ ) in the absence of the TNT. One of the important contributions of this work is the observation that the relative peak area decrease with the amount of added TNT to the solution. The measurements showed that the fluorescence intensity was proportional to the concentration of the quantum dots in solution. The fluorescence of the QDs is quenched by the added TNT. They found that the TNT doesn't have an effect on the size of the QD. The schemes below show the mechanism of charge transfer between TNT and the QD that they proposed.



Scheme 6.1 and 6.2: Charge transfer process between TNT and quantum dots.

They proposed a charge transfer process between TNT and quantum dots and/or the involvement of the new trap states (NTS) in the fluorescence emission of the dots. Here, we extend this concept to detect cardiac serum in the samples of the blood serum of real patients.

### 6.1.3 Sensing applications of nanoparticles in biological and biomedical systems

Xiaohu Gao and Shuming Nie, studied the applications of nanoparticles in biology and medicine<sup>18</sup>. Living organisms are built of cells that are typically 10  $\mu\text{m}$  across. Cell parts are much smaller and are in the sub-micron size domain. Even smaller are the proteins with a typical size of just 5 nm, which is comparable to the dimensions of smaller man made nanoparticles. This simple size comparison gives an idea of using nanoparticles as very small probes that would allow us on spy at the cellular machinery without introducing too much interference. Some of the applications of nanomaterials to biology or medicine are fluorescent biological labels, drug and gene delivery, bio detection of pathogens, detection of proteins, probing of DNA structure, tissue engineering, tumor destruction via heating (hyperthermia), separation and purification of biological molecules and cells, MRI contrast enhancement and phagokinetic studies. Single quantum dots of compound semiconductors were successfully used as a replacement of organic dyes in various bio-tagging applications. This idea has been taken one step further by combining differently sized nanoparticles and hence having different fluorescent color quantum dots, and combining them in polymeric microbeads. A precise control of quantum dot ratios has been achieved. The selection of nanoparticles used in those experiments had 6 different colors as well as 10 intensities. It is enough to encode over 1 million combinations. The uniformity and reproducibility of beads was high, allowing bead identification accuracies of 99.99%. Gold nanoparticles are widely used in immunohistochemistry to identify protein-protein interaction. The group of Prof. Mirkin<sup>19</sup> has designed a sophisticated multifunctional probe that is built around a 13 nm gold nanoparticle. The nanoparticles are coated with hydrophilic oligonucleotides containing a Raman dye at one end and terminally capped with a small molecule recognition element (e.g. biotin). Moreover, this molecule is catalytically active and

coated with silver in the solution of Ag (I) and hydroquinone. Apart from being able to recognize small molecules this probe can be modified to contain antibodies on the surface to recognize proteins. When tested in the protein array format against both small molecules and proteins, the probe has shown no cross-reactivity.

Sharron G. Penn et al studied nanoparticles for bioanalysis<sup>20</sup>. Nanotechnology is having an impact in bioanalysis, where nanoparticles of a variety of shapes, sizes and compositions are poised to fundamentally change the bioanalytical measurement landscape. Nanoparticles will overcome many of the significant chemical and spectral limitations of molecular fluorophores. Nanoparticles as quantization tags in biological assays are used in order to eliminate the need of either organic fluorophores or radioactive labeling. The work was based in quantum dots and metallic nanoparticles. Quantum dots take advantage of the quantum confinement effect, giving the nanoparticles unique optical and electronic properties. Quantum dots offer advantages over conventional dye molecules in that they have tunable fluorescence signatures, narrow emission spectra, brighter emission and good photostability.

An active research in the development of surface coatings can be derivatized with biomolecules without changing the optical properties of the quantum dots. Other works are based in the attempt to derivatize colloidal gold with biomolecules. The use of quantum dots as fluorescent probes in biological applications has become a reality. Different groups are studying her 2 assay for breast cancer, imaging of cell mobility, and in vivo mouse lung targeting between others. Encoded nanoparticles can serve as substrates for multiplexed biological assays in solution. Compared with microarray based methods, these suspensions offer greater flexibility, more rapid assay times, greater reproducibility, and can potentially use less sample and reagent.

Also, nanoparticles can act as signal transducers, showing the most promise in diagnostic assays, due to the elimination of the need to tag biological sample. Nanoparticles will become valuable for bioanalysis when protocols involving them become widely adopted.

Xiaohu Gao and Shuming Nie studied the molecular profiling of single cells and tissue specimens with quantum dots<sup>21</sup>. Traditional fluorophores suffer from several problems, such as photobleaching, spectral cross talking and narrow excitation. Quantum dots have the potential to overcome these problems. These results suggest that multicolor quantum dots could be used to determine the quantitative profiles of molecular targets for single normal or diseased cells. The improved brightness and photostability are also important for detection and identification of low-abundance antigens that are present in only 10-100 copies per cell. Another application of quantum dots is in multiplex labeling and molecular analysis of pathological tissue specimens. Clinical tissue specimens are often highly heterogeneous and are more difficult to analyze. Quantum dots coupled with spectroscopy and spectral imaging could have an important role in mapping out the true molecular profiles associated with different diseases. The recent development of near infrared emitting quantum dots and quantum dot encoded beads should allow molecular profiling of a large number of genes, proteins and other biomolecules on a single tissue section.

P.O. Collinson and P.J Stubbs studied troponins<sup>22</sup>. Cardiospecificity and sensitivity of cardiac troponin measurement has produced a paradigm shift in the assessment of patients with suspected acute coronary syndromes. There are other causes of troponin release, elevations are specific for cardiac damage but cardiac damage does not equate myocardial infarction. Troponin elevation is an independent mortality predictor. Measurement of cardiac troponin provides a

sensitive diagnostic test when it is used together with other information. Current assays are unable to detect troponin in the majority of normal healthy individuals. The situation may be improved by more sensitive assays.

M. Plebani et. al, studied the quality specifications for biochemical markers of myocardial injury<sup>23</sup>. In the diagnosis and monitoring of myocardial damage, the role of biochemical markers, in particular troponins, demonstrated that all elevated values were associated with a worsened prognosis. This article focused on how the application of quality specifications may be useful in order to provide advice to clinicians in their investigations of complex clinical cases of patients suffering from myocardial damage. They examined samples of three patients admitted to the hospital with symptoms suggestive of a cardiac disease. The troponin I high values did not correlate with clinical condition, which was investigated to verify the accuracy of the laboratory data. They evaluated the relation between the standard of quality specifications and the assay specificity, imprecision and interferences. They demonstrated that the cases of false positive cTnI values could be attributed to a macrocomplex between a modified in vivo cTnI and immunoglobulin G (case 1) and to the presence of heterophilic antibodies affecting the RxL Dimension procedure (case 3). The lack of standardization as well as the wide differences in the development of each assay gives rise to major concerns regarding cTnI determinations. The authors recommended laboratories to check the compliance between analytical characteristics of the method utilized against quality specifications for a better understanding of the frequency of false positive results as well as other serious errors.

New methodologies for glucose sensing using gold and silver nanoparticles are based on the specific biological interactions between Con A, dextran-coated gold nanoparticles and glucose, and the interactions between dextran, glucose and boronic acid capped silver nanoparticles in

solution. Dextran coated gold nanoparticles were aggregated with the addition of Con A resulting in an increase in absorbance of nanoparticles at 650nm. The post addition of glucose caused a dissociation of the aggregates and a decrease in the absorbance at 640nm. The interaction of glucose and dextran with boronic acid-capped silver nanoparticles in solution resulted in enhanced luminescence intensity cumulatively due to surface enhanced fluorescence and the decrease in absorbance at 440nm, with an increase in absorbance at 640nm<sup>13</sup>.

#### **6.1.4 Nanotechnology for sensing cardiac failure biomarkers**

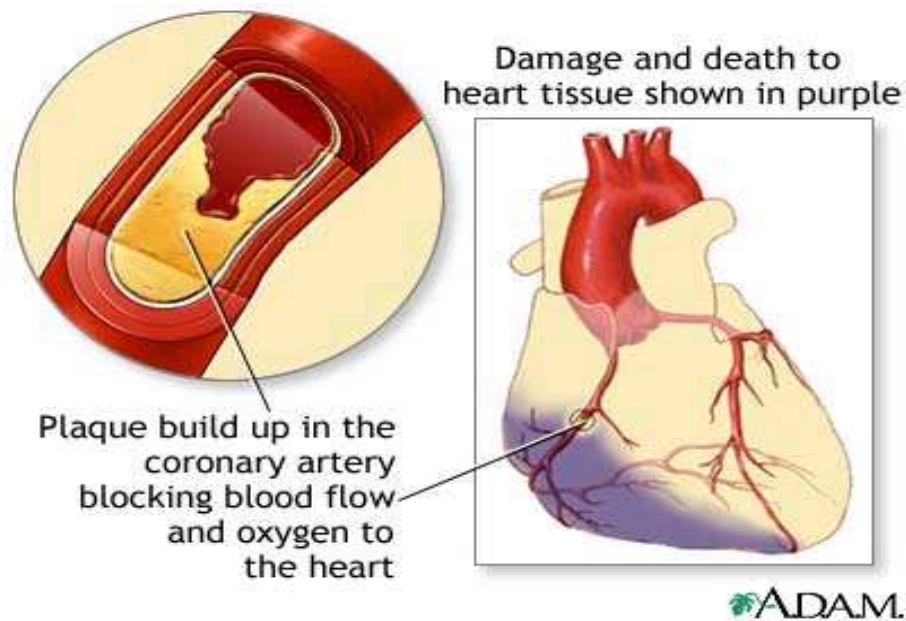
There are a few scattered studies on the use of nanotechnology for sensing biomarkers associated with cardiac failure that have appeared in the literature after our work was initially published in the Puerto Rico Health Science Journal issue of September of 2009. In a report that will appear in the January 2011 issue of the Journal of Biosensors and Bioelectronics, Innam Lee and co-workers used a single polyaniline (PANI) nanowire-based biosensor to detect immunoglobulin G (IgG) and myoglobin (Myo). The target proteins of IgG and Myo were detected by measuring the conductance change of functionalized single PANI nanowires owing to the capturing of target proteins by mAbs. The detection limit was found to be 3 ng/mL for IgG and 1.4 ng/mL for Myo<sup>24</sup>.

In the March 2010 issue of Sensors and Actuators, Wen-Ya Wu and collaborators studied poly(dimethylsiloxane) (PDMS)-gold nanoparticles (AuNPs) composite film as a tool to enhance the colorimetric detection of cardiac troponin I (cTnI). These authors found that the proposed colorimetric method was yielded similar results to the enzyme-linked immunosorbent assay (ELISA) for cTnI detection in clinical samples<sup>25</sup>. In a report that appeared in the January 2010 issue of the Journal of Biosensors and Bioelectronics Dong Hwan Choi and coworkers, on the

other hand, developed a new and simple method using two AuNP-antibody conjugates for signal amplification without an additional operation step in a gold nanoparticle (AuNP)-based lateral flow assay (LFA). They detected as low as 0.01 ng/mL troponin I in 10 min using the dual AuNP conjugate-based LFA, which was successfully applied in the analysis of serum samples of patients with myocardial infarction<sup>34</sup>.

## **6.2 Justification**

Each year, about 1.1 million people in the United States have heart attacks, and almost half die. Heart attacks occur most often as a result of a condition called coronary artery disease (CAD). It is the leading killer disease of both men and women in the United States. Heart disease is caused by narrowing of the coronary arteries that feed the heart. Like any muscle, the heart needs a constant supply of oxygen and nutrients, which are carried to it by the blood in the coronary arteries. When the coronary arteries become narrowed or clogged by cholesterol and fat deposits, a process known as atherosclerosis occurs. When not enough blood is supplied to the heart, the result is coronary heart disease (CHD). If not enough oxygen-carrying blood reaches the heart, a chest pain, called angina, will develop. If the blood supply to a portion of the heart is completely cut off by total blockage of a coronary artery, the result is a heart attack. This is usually due to a sudden closure from a blood clot forming on top of a previous narrowing. Figure 6.1 show an illustration of a heart damage caused by a CAD.



Approximately half of these deaths occur within one hour of the start of symptoms and before the person reaches the hospital. About 57% of men and 64% of women that suffer sudden death by cardiovascular diseases do not exhibit certain physical characteristics such as chest pain, unusual fatigue and sleep disturbance easily associated with heart failure.

### **6.3 General Background**

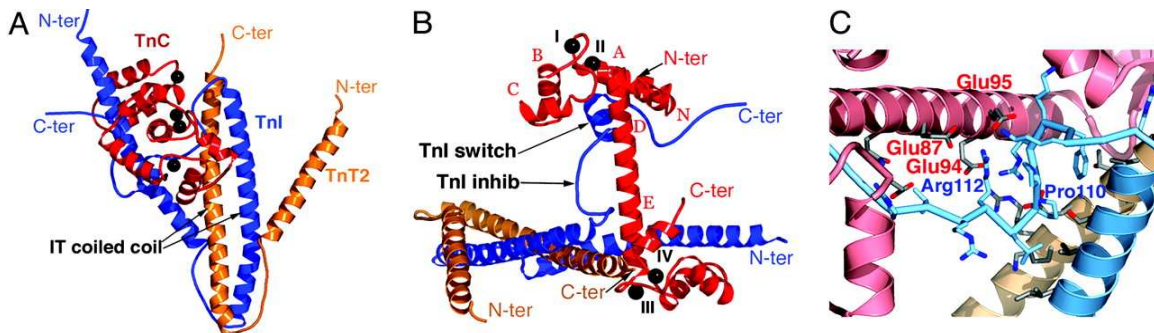
Different biomarkers such as CK-MB, myoglobin and troponin are used to diagnose heart failure. In table 6.1 is presented a summary of the different biomarkers and their application.

Marker	What is?	Tissue Source	Reason for increase	Time to increase	Time back to normal	When/how used
CK	Enzyme - three different isoenzymes exist	Heart, brain, and skeletal muscle	Injury to muscle and/or heart cells	4 to 6 hours after injury, peaks in 18 to 24 hours	48 to 72 hours, unless due to continuing injury	Performed in combination with CK-MB
CK-MB	Heart-related isoenzymes of CK	Heart primarily, but also in skeletal muscle	Injury to heart and/or muscle cells	4 to 6 hours after heart attack, peaks in 12 to 20 hours	24 to 48 hours, unless new or continuing damage	Less specific than troponin, may be ordered when troponin is not available
Myoglobin	Oxygen-storing protein	Heart and other muscle cells	Injury to muscle and/or heart cells	2 to 3 hours after injury, peaks in 8 to 12 hours	Within one day after injury	Sometimes performed with troponin to provide early diagnosis
Cardiac Troponin	Regulatory protein complex. Two cardiac-specific isoforms: T and I	Heart	Injury to heart	4 to 8 hours	Remains elevated for 7 to 14 days	Diagnose heart attack, assess degree of damage

Table 6.1 Common Cardiac Biomarkers

Reference: ©2001 - 2011 by American Association for Clinical Chemistry

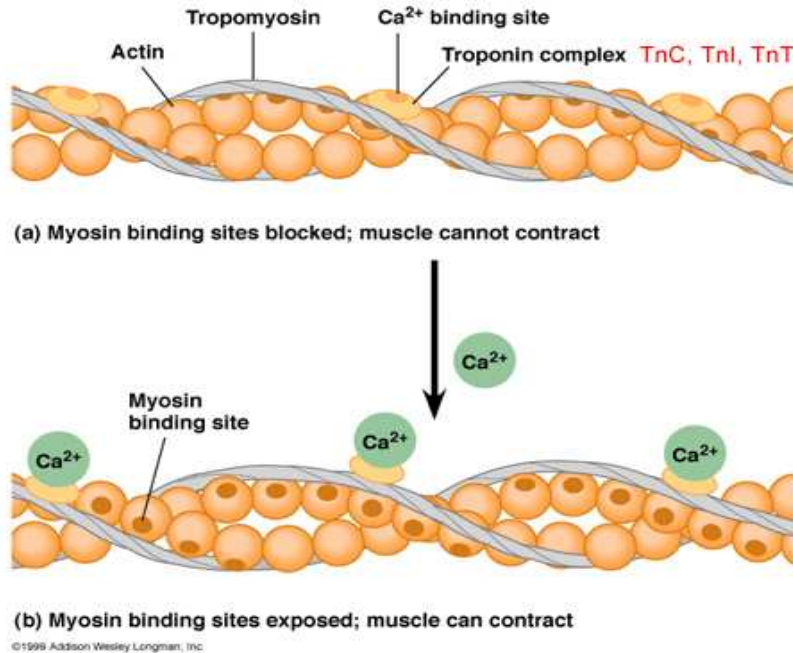
Studies related to cardiovascular diseases show that troponin is an excellent biological marker for cardiovascular diseases. Troponin is a complex consisting of three proteins that play a central role in skeletal and cardiac muscle contraction. It has three subunits, known as troponin C, which fixes  $Ca^{2+}$ , troponin I, an inhibitor of actin-myosin interaction, and troponin T, which is attached to a protein called tropomyosin. It lies within the groove between actin filaments in muscle tissue. In a relaxed muscle, tropomyosin prevents contraction by blocking the attachment site for myosin crossbridge.



Biochemistry (Moscow), Vol. 64, No. 9, 1999, pp. 969-985

Figure 6.2: Structure of skeletal troponin complex presented in two orientations. The troponin subunits are color-coded as follows: orange, TnT2; blue, TnI; and red, TnC. Black spheres indicate Ca. The termini of subunits are shown and color-coded as described above. (A) The nearly twofold symmetrical assembly of TnI and TnT2 subunits. The rotation angle that would create the best match between the subunits is  $\approx 174^\circ$ . (B) The TnC central helix is orientated perpendicular to the plane of TnI and TnT2. The capital-letter coding in red corresponds to the TnC helices in the N-terminal regulatory domain and for the central linker. The TnI inhibitory and switch segments are indicated. Roman numerals indicate the  $\text{Ca}^{2+}$ -binding sites. (C) Close-up view of the TnI inhibitory segment. The residues determining the position of the TnI inhibitory segment are shown as stick models. The colors in this image are faded to avoid confusion with the red and blue oxygens and nitrogens in the stick models.

A fraction of the calcium released when a muscle contraction is stimulated attaches to the troponin, resulting in a conformational change that result in muscle contraction. When cells from the myocardiac tissue loose membrane integrity, the intracellular molecules diffuse into the microcirculation and linfatics. These molecules are found in the circulation and constitute the specific biological markers of myocard tissue damage.



Biochemistry (Moscow), Vol. 64, No. 9, 1999, pp. 969-985

Figure 6.3: A model of the molecular arrangement of troponin (Tn), tropomyosin (Tm), and actin in the cardiac muscle thin filament.

Troponin is released into the human blood stream after heart damage occurs, as described in the previous paragraph, a few hours prior to a heart attack. Early troponin detection provides a useful tool for the detection of coronary disease a few hours before a major heart attack. Indeed, clinical testing of heart failure based on troponin detection has found widespread use over other cardiac biomarkers, like creatine phosphokinase (CK), creatine kinase (CK-MB) and myoglobin testing.

#### 6.4 Objective of proposed research

Nanotechnology may represent a tool for the improvement in our quality of life by providing a platform for new sensors or sensing elements – components that can be integrated into functional sensors- to monitor chemicals closely related to health issues. A sensor is a device that receives and responds to a signal or stimulus indicative of a physical condition. The aim of

the work presented here is to evaluate the response of CdS semiconductor nanoparticles on the serum of patients that have been evaluated for cardiac troponin, a protein that has been the subject of previous works related to its value in the prognosis, risk stratification and management of patients with acute coronary syndromes and myocardial necrosis<sup>26-30</sup>. These are major health issues, costing consumers millions of dollars through high insurance premiums and health care. Development of a real time sensor that targets the detection of cardiac troponin in the blood is a major technological challenge that can reduce mortality and health care costs.

In a typical semiconductor, electrons can be excited by light from the valence band into the conduction band. The minimum energy required to promote electrons from the valence band into the conduction band represents the band gap of the semiconductor, which is inversely proportional to the nanoparticle size<sup>31</sup>. Photo-excited electrons in the conduction band are energetically relaxed to lower energy states or traps, which are states resulting from defects in the structure of the nanoparticle or from the adsorption of chemicals on their surface. Emission of light results from relaxation of electrons from trap states into the valence band. When the trap states arise from the adsorption of molecules on the particle surface, the resulting luminescence is very sensitive to the chemical environment of the semiconductor nanoparticle: a potential sensor element to the specific chemical that created the trap state.

## **6.5 Methodology**

### **Synthesis of CdS Nanoparticles and serum sample selection**

The synthesis of CdS fluorescent nanoparticles was achieved using  $\text{Cd}(\text{CH}_3\text{CO}_2)_2$  as a convenient source of  $\text{Cd}^{+2}$  ions to form the CdS NP in dimethylsulfoxide (DMSO) in a microwave oven. A detail explanation of NP synthesis method is provided in Chapter 5. The

interaction of the synthesized CdS nanoparticles with serum blood samples was studied measuring changes in the optical properties (absorption and emission) of the nanoparticles. Serum samples are a yellow colored liquid in which the blood cells are suspended. Typical serum samples composition are 92% water, 6-8% proteins, 0.8% of salts, 0.6% of lipids and 0.1% of glucose. Figure 6.3 show a typical human blood serum sample. We worked with cardiac and non cardiac patients serum samples provided by Hospital Perea Clinical Laboratory at Mayaguez, P.R. Photoluminescence measurements were performed in a Shimadzu 5301 Spectrofluorimeter instrument with a 30 second data acquisition time.

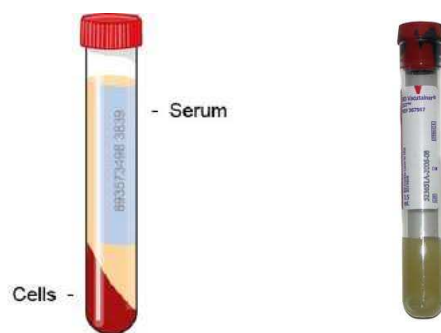


Figure 6.4 Human Blood Serum

## 6.6 Results and Discussion

The inset in figure 6.5 shows the absorbance spectrum of the CdS nanoparticles in dimethylsulfoxide (DMSO) employed for the work described here. The absorbance decreases with wavelength until the band edge of the semiconductor nanoparticle is reached around 515 nm. Based on the absorbance cutoff it is possible to estimate a nanoparticle diameter of about 2.4 nm<sup>30</sup>. Serum samples of patients obtained from the Hospital Perea Clinical Laboratory were analyzed for cardiac troponin levels using the Abbott method [the AxSYM Troponin-I assay , a

microparticle enzyme immunoassay, is a two-site assay that uses an anti-cTnI monoclonal antibody for capture and a polyclonal anti-cTnI antibody for detection].<sup>32</sup>

A typical emission spectrum of a solution prepared by adding 90  $\mu\text{L}$  of the serum of a patient with no detectable cardiac troponin to a 1 mL of a solution containing the approximately  $1.5 \times 10^{12}$  CdS nanoparticles is labeled as Patient 1 in figure 6.5. No new emission bands besides those associated with the emission of the CdS nanoparticle appear in the spectrum. On the other hand, the photoluminescence of a mixture containing CdS nanoparticles and 90  $\mu\text{L}$  of serum of a patient with a troponin level of 1.8 mg/mL, labeled as patient 2 on figure 6.5, exhibit bands around 545 nm a low wavelength shoulder between 500 and 540 nm and a high wavelength peak around 580 nm. Figure 6.6 summarizes the photoluminescence spectra as a function of troponin concentration in serum-CdS NP assays examined in patient 2 and illustrates the reproducibility of the assay.

The insert in figure 6.5 summarizes the photoluminescence intensity as a function of troponin concentration in three different patients. The emission light intensity decreases linearly with dilution in the serum samples examined indicating that the emission is from the mixture and not an experimental artifact. Control experiments with troponin containing serum do not show these bands in the absence of the CdS particles. A lower detection limit of about 54 nanograms/mL is estimated from the measurements. Smaller detection limits have been attained using other nano-based sensing platforms at the expense of the use of data collection times longer than those used by us in this work.

The number and chemical nature of other biomarkers that may be present in the serum samples limits the interpretation of the results in terms of specific troponin-CdS nanoparticle interaction<sup>33-34</sup>. However, the results encourage pursuing further work focused on the use of CdS

nanoparticles for the detection of cardiac troponin and other biomarkers related to coronary syndromes.

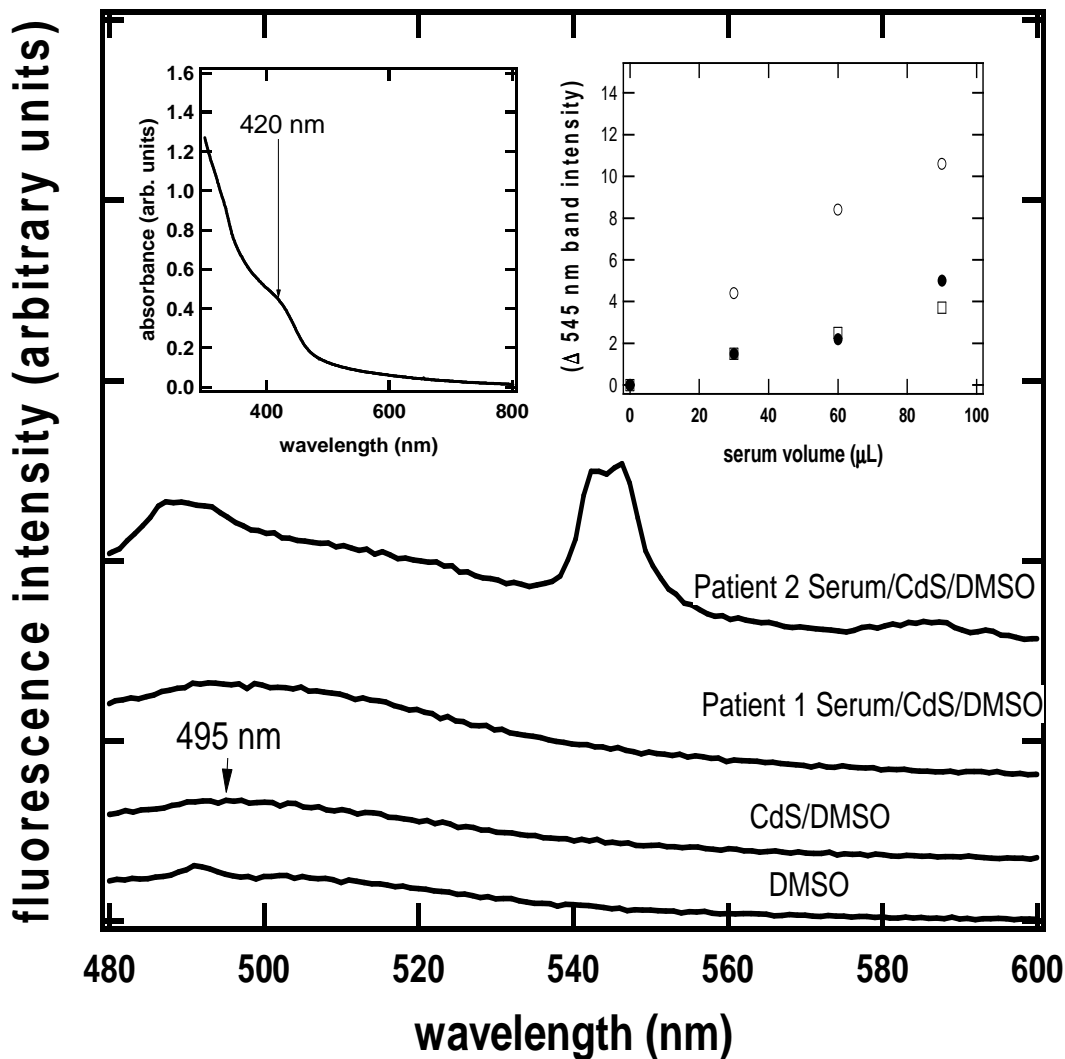


Figure 6.5: The inset at the upper left hand side shows a typical absorption spectrum of CdS nanoparticles. The fluorescence spectra of DMSO, the CdS nanoparticles in DMSO, the serum of patients with no detectable troponin (patient 1), and of a patient containing 1.8 mg/mL of troponin in serum (patient 2). Excitation wavelength is 420 nm in all fluorescence measurements. The inset at the right hand side shows the change in fluorescence intensity at 545 nm as a function of the serum volume of patients with troponin levels of 15 (open circles), 12 (closed circles) and 2 (open squares) mg/mL.

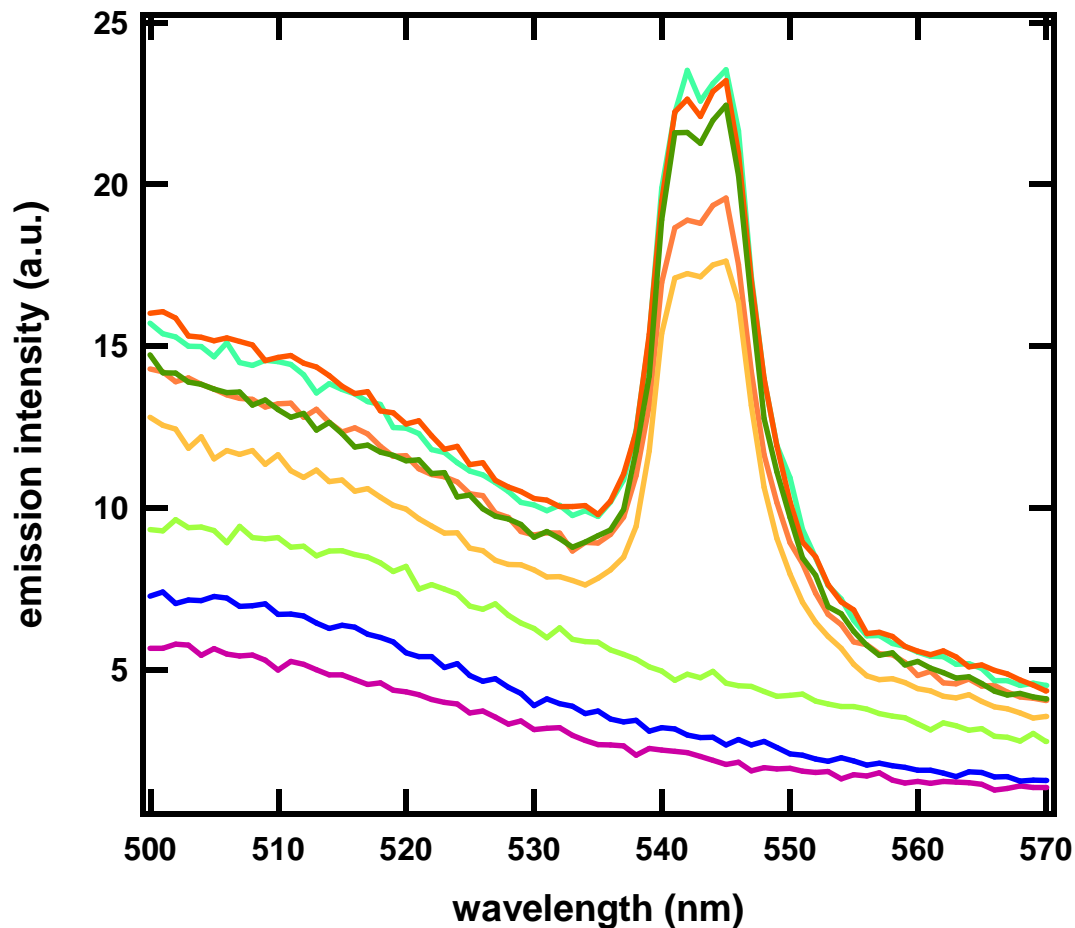


Figure 6.6: Show the emission intensity of a concentration profile for 1.8mg troponin serum of cardiac patient. Addition of 30  $\mu\text{L}$ , 45 $\mu\text{L}$ , 60 $\mu\text{L}$  and 90 $\mu\text{L}$  to 1mL of a solution containing approximately  $1.5 \times 10^{12}$  CdS nanoparticles were performed. Figure show the increase in emission intensity as a function of cardiac patient serum concentration.

## 6.7 Acknowledgement

EF acknowledges a PhD scholarship from the Sloan Foundation and a scholarship from Puerto Rico Industrial Development Company (PRIDCo). FZ and ET acknowledge undergraduate student scholarships from the UPRM Biominds Program and the National Institute of Health

Minority Access to Research Careers (MARC) Program. Partial financial support from Dupont Electronic Technologies and the UPRM Department of Chemistry is gratefully acknowledged.

## 6.8 References

1. Prashant V. Kamat.; Photophysical, Photochemical and Photocatalytic aspects of metal nanoparticles. **2002**. *J.Phys.Chem. B* 106; 7729-7744.
2. Kittel C.; Introduction to Solid State Physics. Seven Edition. *Jon Wiley & Sons*. **1996**.
3. Thelma Serrano, Idalia Gomez, Rafael Colas, Jose Cavazos.; Synthesis of CdS nanocrystals stabilized with sodium citrate. *Eng.Aspects* **2009**: 338 20-24.
4. V.P. Singh, R.S. Singh, G.W. Thompson, V. Jayaraman, S. Sanagapalli, V.K. Rangari. Characteristics of nanocrystalline CdS films fabricated by sonochemical methods for solar cell applications. *Solar Energy Materials and Solar Cells* **2004**: 81 293-303
5. G.Z. Wang, W.Chen, C.H. Liang, Y.W.Wang, G.W. Meng and L.D. Zhang.; Preparation and characterization of CdS Nanoparticles by ultrasonic radiation. *Inorganic Chemistry Communications* **2001**: 4(1) 208-210.
6. S. Martinez, T. Serrano, I. Gomez, A. Hernandez.; Synthesis and Characterization of CdS nanoparticles by microwave irradiation. *Bol.Soc.Esp.Ceram.* **2007**: 46(2) 97-101.
7. C. Unni, Daizy Philip, S.L. Smitha, K.M. Nissamudeen, K.G. Gopchandran.; Aqueous synthesis and characterization of CdS, CdS:Zn<sup>2+</sup> and CdS:Cu<sup>2+</sup> quantum dots. *Spectrochimica Acta Part A:Molecular and Biomolecular Spectroscopy* **2009**: 72(4) 827-832.
8. Manoj E. Wankhede, Santosh K. Haram.; Synthesis and Characterization of Cd- DMSO Complex Capped CdS Nanoparticles. *Chem.Mater* **2003**: 15 1296-1301.
9. N. Revaprasadu, S.N. Mlondo.; Use of metal complexes to synthesize semiconductor nanoparticles. *Pure Appl.Chem.* **2006**: 78(9) 1691-1702.
10. P.K. Khanna and Narendra Singh.; Light emitting CdS quantum dots in PMMA: Synthesis and optical studies. *J. of Luminescence* **2007**: 127 474-482.
11. Junjie Zhu, Miaogao Zhou, Jinzhong Xu and Xuehong Liao.; Preparation of CdS and ZnS nanoparticles using microwave irradiation. *Materials Letters* **2001**: 47, 25-29.

12. Liang Li, Huifeng Qian and Jicun Ren.; Rapid synthesis of highly luminescent CdTe nanocrystals in the aqueous phase by microwave irradiation with controllable temperature. *Chem. Commun.*, **2005**, 528–530
13. Aslan K.; Saccharide Sensing Using Gold and Silver Nanoparticles. **2004**. *Journal of Fluorescence* 14(4); 391.
14. Geddes, C.; Luminescent Blinking from Noble-Metal Nanostructures: New Probes for Localization and Imaging. **2003**. *Chemical Physics Letters*. 380; 269-272.
15. Mock J.J. et al.; Shape effects in plasmon resonance of individual colloidal silver nanoparticles. **2002**. *Journal of Chemical Physics*. 116(15); 6755-6759.
16. Gammon D.; Optical Studies of Single Quantum dots. **2002**. *Physics Today*. 55(10); 36-42.
17. S.Nieto et al. Nanoscaled Science and Engineering for Sensing: Quantum Dots Fluorescence Quenching for Organic NO<sub>2</sub> Sensing. **SPIE 2004**.
18. Xiaohu Gao.; Moleccular profiling of single cells and tissue specimens with quantum dots. **2003**. *Trends in Biotechnology* 21(9): 271
19. Salata, OV. Applications of nanoparticles in biology and medicine. *Journal of Nanobiotechnology*, **2004**, 2, 1-6.
20. Penn S.H., Nanoparticles for bioanalysis. **2003**. *Chemical Biology* 7; 609-615.
21. Xiaohu Gao.; In vivo cancer targeting and imaging with semiconductor quantum dots. **2004**. *Nature Biotechnology*. 22(8); 969.
22. Collinson P.O., Are Troponins Confusing. **Nov.2003**. *Heart* 89(11); 1285.
23. Plenbani, M.; Quality Specifications for biochemical markers of myocardial injury. **2004**. *Clinica Chemica Acta* 346 65-72.
24. Lee, I., Luo, X., Cui, X.T., Yun, M., Highly sensitive single polyaniline nanowire biosensor for the detection of immunoglobulin G and myoglobin, *Biosensors and Bioelectronics* (2010), doi:10.1016/j.bios.2011.01.001
25. Wu, W.; Bian, Z.; Wei Wang, P.; Wang, W.; Zhu, J. PDMS gold nanoparticle composite film-based silver enhanced colorimetric detection of cardiac troponin. *Sensors and Actuators B*, **2010**,147, 298–303.
26. You JJ, Austin PC, Alter DA , Ko DT, Tu JV. Relation between cardiac troponin I and mortality in acute decompensated heart failure. *American Heart Journal* 2007; 153:462-470.

27. Hentschel D. M., Aviles R. J., Topol E. J., Lauer M. S. Troponin T Levels and Acute Coronary Syndromes. *New Engl J Med.* 2002; 347:1722-1723.
28. Antman EM. Decision Making with Cardiac Troponin Tests. *New England Journal of Med* 2007; 346: 2079-2082.
29. Antman E M, Tanasijevic MJ, Thompson B, Schactman M, McCabe CH, Cannon CP, Fischer GA, Fung AY, Thompson C, Wybenga D, Braunwald E. Cardiac-Specific Troponin I Levels to Predict the Risk of Mortality in Patients with Acute Coronary Syndromes. *New England Journal of Med* 1996; 335(18): 1342-1349.
30. Olatidoye AG, Wu AHB, Feng YJ, Waters D. Prognostic role of troponin T versus troponin I in unstable angina pectoris for cardiac events with meta-analysis comparing published studies. *J. of Cardiology* 1998; 81(12): 1405-1410.
31. Brus LE. Electron-electron and electron-hole interactions in small semiconductor crystallites: The size dependence of the lowest excited electronic state. *The Journal of Chemical Physics* 1984; 80: 4403-4403.
32. Apple, F.; Maturen, A. J.; Mullins, R. E.; Painter, P. C.; Pessin-Minsley, M.; Webster, R. A.; Spray Flores, J.; DeCresce, R.; Fink, D. J.; Buckley, P. M.; Marsh, J.; Ricchiuti, V.; Christenson, R.H. Multicenter Clinical and Analytical Evaluation of the AxSYM Troponin-I Immunoassay to Assist in the Diagnosis of Myocardial Infarction. *Clinical Chemistry*, **1999**, 45, 206–212
33. Braunwald E. Biomarkers in Heart Failure. *New England Journal of Medicine* **2008**; 358:2148-2159.
34. Dong Hwan Choi, Seok Ki Lee, Young Kyoung Oh, Byeong Woo Bae, Sung Dong Lee, Sanghyo Kim, Yong-Beom Shin, Min-Gon Kim. A dual gold nanoparticle conjugate-based lateral flow assay (LFA) method for the analysis of troponin I. *Biosensors and Bioelectronics* 25 (**2010**) 1999–2002
35. Ferrer Torres, Edmy J., Zayas, F., La Torre, E. and Miguel E. Castro. Fluorescence response of CdS nanoparticles to serum of cardiac patients: towards the development of a real time sensor for heart failure detection. *Puerto Rico Health Science Journal* September 2009.

## CHAPTER 7: CONCLUSION

---

The objective of this dissertation was to develop a new method for the synthesis of CdS fluorescent nanoparticles that can facilitate their use as sensor or sensor elements. The formation of CdS nanoparticles was achieved using a method developed here in our laboratory. The work lead to nucleation and growth studies pertaining to nanoparticle formation using microwave radiation as the energy source. Strong evidence was found for the formation of  $(\text{CdS})_{1 < n < 5}$  clusters at the early stages of the process. A mechanism for nuclei formation under the experimental conditions discussed above was presented and discussed. The formation of the clusters and nuclei as well as the growth of CdS NP w`as controlled by turning “on” and “off” the energy supply leading us to conclude that there is an energy barrier to CdS nanostructures formation. The potential of the CdS NP prepared by the method described here to sense cardiac conditions was also established. We established that the fluorescence of the CdS NP changed in the chemical environment of cardiac patients only, opening a new door for further work in the development of a real time sensor for cardiac failure.

## CHAPTER 8: FUTURE WORKS

---

### 1. Functionalization of the fluorescent nanostructures surfaces with monoclonal antibodies: bio inorganic functionalization

The use of the antigen-antibody concept to detect cardiac biomarkers will be a great future work. Functionalization of the fluorescent nanostructure surfaces with monoclonal antibodies to cardiac troponin must be a great future work. There are a wide variety of antibodies to cardiac troponin that includes mouse antibody, goat antibody and rabbit antibody. Serum samples may be exposed to antibody-CdS NP ensemble in a matrix or in solution. Since the troponin antibody is specific to troponin it can result in great selectivity in sensing heart failure conditions. The same concept can be extended to other cardiac biomarkers to search for the best antibody-antigen combination to be used with CdS NP based platforms.

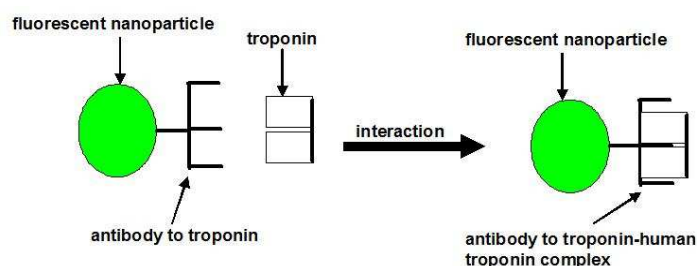


Figure 9: Fluorescent nanoparticle functionalized with antibody selective to troponin bind selectively to human troponin.

### 2. Lifetime of fluorescent nanoparticles bound to troponin

Time dependent measurements of the fluorescence lifetime will also be an attractive approach to sense cardiac biomarkers. In this case one would search for differences in the fluorescence emission lifetime as a function of the cardiac biomarker bound to the nanoparticle surface. The studies are time dependent and can provide a history of the effect of the biomarker on the

electronic excitation process that take place in/on the particle allowing. Are the lifetimes dependent on the nature of the biomarker? Can it be used in a common everyday scenario like a hospital?

### **3. Single molecule spectroscopy and imaging measurements: determination of fluorescence wavelength and**

Near field optical microscopy is ideally suited to study the interaction between the fluorescent nanostructure and troponin. In near field optical microscopy, light can be delivered or collected by a small aperture, smaller than the light wavelength, at the end of a fiber optic. The spatial resolution in the near field is defined by the size of the aperture or point source in the fiber optic (as small as 50 nm). That is a unique capability that allows for a number of light spectroscopy techniques, like absorption, fluorescence and luminescence and vibrational spectroscopy, to be performed. Therefore, the spectroscopic fingerprint in nanostructured materials can be obtained. A great deal of information can be learned about the interaction between proteins and nanostructures, and in the case presented here, will be instrumental in addressing the potential use of fluorescent nanoparticles in sensing troponin and other cardiac biomarkers.

## CHAPTER 9: GENERAL REFERENCES

---

### References Chapter 1-4

1. <http://en.wikipedia.org/wiki/sensor>
2. Ross G., Bever F.N., Uddin ZI and Hockman E.M. "Troponin I sensitivity and specificity for the diagnosis of acute myocardial infarction". January 2000. *JAOA* 100(1); 29-31.
3. Hu J., Odom T.W. and Lieber C. "Chemistry and Physics in one dimension: Synthesis and Properties of nanowires and nanotubes". 1999 *Acc.Chem.Res.* 32; 435-445.
4. Kittel C.; Introduction to Solid State Physics. Seven Edition. *Jon Wiley & Sons.* **1996**.
5. Alvarez MM., Khoury J.T. et al. "Critical sizes in the growth of Au Clusters" February 1997. *Chemical Physics Letters.* 266(9); 1-98.
6. Thelma Serrano, Idalia Gomez, Rafael Colas, Jose Cavazos.; Synthesis of CdS nanocrystals stabilized with sodium citrate. *Eng.Aspects* **2009**: 338 20-24.
7. V.P. Singh, R.S. Singh, G.W. Thompson, V. Jayaraman, S. Sanagapalli, V.K. Rangari. Characteristics of nanocrystalline CdS films fabricated by sonochemical methods for solar cell applications. *Solar Energy Materials and Solar Cells* **2004**: 81 293-303
8. G.Z. Wang, W.Chen, C.H. Liang, Y.W.Wang, G.W. Meng and L.D. Zhang.; Preparation and characterization of CdS Nanoparticles by ultrasonic radiation. *Inorganic Chemistry Communications* **2001**: 4(1) 208-210.
9. S. Martinez, T. Serrano, I. Gomez, A. Hernandez.; Synthesis and Characterization of CdS nanoparticles by microwave irradiation. *Bol.Soc.Esp.Ceram.* **2007**: 46(2) 97-101.
10. C. Unni, Daizy Philip, S.L. Smitha, K.M. Nissamudeen, K.G. Gopchandran.; Aqueous synthesis and characterization of CdS, CdS:Zn<sup>2+</sup> and CdS:Cu<sup>2+</sup> quantum dots. *Spectrochimica Acta Part A:Molecular and Biomolecular Spectroscopy* **2009**: 72(4) 827-832.
11. Manoj E. Wankhede, Santosh K. Haram.; Synthesis and Characterization of Cd- DMSO Complex Capped CdS Nanoparticles. *Chem.Mater* **2003**: 15 1296-1301.
12. N. Revaprasadu, S.N. Mlondo.; Use of metal complexes to synthesize semiconductor nanoparticles. *Pure Appl.Chem.* **2006**: 78(9) 1691-1702.
13. P.K. Khanna and Narendra Singh.; Light emitting CdS quantum dots in PMMA: Synthesis and optical studies. *J. of Luminescence* **2007**: 127 474-482.

14. Junjie Zhu, Miaogao Zhou, Jinzhong Xu and Xuehong Liao.; Preparation of CdS and ZnS nanoparticles using microwave irradiation. *Materials Letters* **2001**: 47, 25-29.
15. Liang Li, Huifeng Qian and Jicun Ren.,; Rapid synthesis of highly luminescent CdTe nanocrystals in the aqueous phase by microwave irradiation with controllable temperature. *Chem. Commun.*, **2005**, 528–530
16. Prashant V. Kamat.; Photophysical, Photochemical and Photocatalytic aspects of metal nanoparticles. **2002**. *J.Phys.Chem. B* 106; 7729-7744.
17. Aslan K.; Saccharide Sensing Using Gold and Silver Nanoparticles. **2004**. *Journal of Fluorescence* 14(4); 391.
18. Murphy, C. J.; Copper, J. L. Quantum Dots: A Primer. *Appl. Spectrosc.* **2002**, 56, 16A-36A.

## References Chapter 5

1. R Bhattacharya, S.Saha.; Growth of CdS nanoparticles by chemical method and its characterization. *Journal of Physics* **2008**: 71(1) 187-192.
2. Jun Zhang, Lingdong Sun, Chunsheng Liao, Chunhua Yan.; Size Control and photoluminescence enhancement of CdS nanoparticles prepared via reverse micelle method. *Solid State Communication* **2002**: 124 45-48.
3. Tiziana Di Luccio, Anna Maria Laera, Leander Tapfer, Susanne Kempter, Robert Kraus, Bert Nickel.; Controlled Nucleation and Growth of CdS Nanoparticles in a Polymer Matrix. *J.Phys.Chem.B* **2006**: 110 12603-12609.
4. Diaz, David, Mario Rivera, Tong Ni, Juan Carlos Rodriguez, Silvia-Elena Castillo-Blum, Dattatri Nagesha, Juvencio Robles, Octavio-Jaime Alvarez-Fregoso, and Nicholas A. Kotov.; Conformation of Ethylhexanoate Stabilizer on the Surface of CdS Nanoparticles. *J.Phys. Chem B* **1999**: 103 9854-9858.
5. V.P. Singh, R.S. Singh, G.W. Thompson, V. Jayaraman, S. Sanagapalli, V.K. Rangari. Characteristics of nanocrystalline CdS films fabricated by sonochemical methods for solar cell applications. *Solar Energy Materials and Solar Cells* **2004**: 81 293-303.
6. Manoj E. Wankhede, Santosh K. Haram.; Synthesis and Characterization of Cd- DMSO Complex Capped CdS Nanoparticles. *Chem.Mater* **2003**: 15 1296-1301.

7. N. Revaprasadu, S.N. Mlondo.; Use of metal complexes to synthesize semiconductor nanoparticles. *Pure Appl.Chem.* **2006**: 78(9) 1691-1702.
8. P.K. Khanna and Narendra Singh.; Light emitting CdS quantum dots in PMMA: Synthesis and optical studies. *J. of Luminescence* **2007**: 127 474-482.
9. U. Resh, A. Eychmuller, M. Haase and H. Weller. ; Absorption of Fluorescence Behavior of Redispersible CdS Colloids in Various Organic Solvents. *Langmuir* **1992**: 8 2215- 2218.
10. Nima Taghavinia, Azam Iraj-zad, S. Mohammad Mahdavi and M. Reza-esmaili. ; Photo-induced CdS nanoparticles growth. *Physica E* **2005**: 30 114-119.
11. Kenneth S. Suslick. ; Sonochemistry. *Science\_* (**1990**): 247 (4949) 1439-1445.
12. Liang Li, Huifeng Qian and Jicun Ren.,; Rapid synthesis of highly luminescent CdTe nanocrystals in the aqueous phase by microwave irradiation with controllable temperature. *Chem. Commun.*, **2005**, 528–530
13. S. Martinez, T. Serrano, I. Gomez, A. Hernandez.; Synthesis and Characterization of CdS nanoparticles by microwave irradiation. *Bol.Soc.Esp.Ceram.* **2007**: 46(2) 97-101.
14. Junjie Zhu, Miaogao Zhou, Jinzhong Xu and Xuehong Liao.; Preparation of CdS and ZnS nanoparticles using microwave irradiation. *Materials Letters* **2001**: 47, 25-29.
15. Privman, V. Diffusional Nucleation of Nanocrystals and Their Self-Assembly into Uniform Colloids. *J. Optoelectronics Adv. Mater.* **2008**, 10, 2827-2839.
16. Wang, C. X.; Yang, G. W. Thermodynamics of Metastable Phase Nucleation at the Nanoscale. *Mat. Sci. Eng. R* **2005**: 49, 157-202.
17. Tobler, D. J.; Shaw, S.; Benning, L. G. Quantification of Initial Steps of Nucleation and Growth of Silica Nanoparticles: An *in-situ* SAXS and DLS Study. *Geochim. Cosmochim. Ac.* **2009**, 73, 5377-5393.
18. Abe´cassis, B.; Testard, F.; Spalla, O.; Barboux, P. Probing In Situ the Nucleation and Growth of Gold Nanoparticles by Small-Angle X-ray Scattering. *Nano Lett.* **2007**: 7, 1723-1727.
19. Rivka Elbaum, Shimon Vega, Gary Hodes.; Preparation and Surface Structure of Nanocrystalline Cadmium Sulfide Precipitated from Dimethyl Sulfoxide Solutions. *Chem.Mater* **2001**: 13 2272-2280.

20. Roman Gajda, Andrzej Katrusiak.; Electrostatic Matching versus Close-Packing Molecular Arrangement in Compressed Dimethyl Sulfoxide (DMSO) Polymorphs. *J.Phys.Chem.B* **2009**: 113 2436-2442.
21. Hongxia Zeng, Raji Reddy Vanga, Dennis S. Marynick, and Zoltan A. Schelly, "Cluster Precursors of Uncapped CdS Quantum Dots via Electroporation of Synthetic Liposome. Experiments and Theory" *J. Phys. Chem. B* **2008**: 112, 14422–14426.
22. E. Caponetti, L. Pedone, D. Chillura Martino, V. Panto , V. Turco Liveri. ; Synthesis, size control, and passivation of CdS nanoparticles in water/AOT/n-heptane microemulsions. *Materials Science and Engineering C* **2003**: 23 531–539.
23. Minjie Li, Jianying Ouyang, Christopher I. Ratcliffe, Laetitia Pietri, Xiaohua Wu, Donald M. Leek, Igor Moudrakovski, Quan Lin, Bai Yang, and Kui Yu, ACS Nano, CdS Magic-Sized Nanocrystals Exhibiting Bright Band Gap Photoemission *via* Thermodynamically Driven Formation **2009**: 3(12), p.3832 – 3838.
24. Ferrer Torres, Edmy J., Rivera D., Gonzalez, Miguel and Miguel E. Castro. Turning "ON"and "OFF" nucleation and growth: microwave assisted síntesis of CdS Clusters and nanoparticles. Accepted in December 2010 in *Materials Research Bulletin*.

### Additional References

- C. Unni, Daizy Philip, S.L. Smitha, K.M. Nissamudeen, K.G. Gopchandran.; Aqueous synthesis and characterization of CdS, CdS:Zn<sup>2+</sup> and CdS:Cu<sup>2+</sup> quantum dots. *Spectrochimica Acta Part A:Molecular and Biomolecular Spectroscopy* **2009**: 72(4) 827-832.
- W.Ronald Fawcett, Alla A. Kloss.; Solvent-Induced Frequency Shifts in the Infrared Spectrum of Dimethyl Sulfoxide in Organic Solvents. *J.Phys.Chem.* **1996**: 100 2019-20-24.
- Yanhong Zhang, Yongming Chen, Haijun Niu, Mingyuan Gao.; Formation of CdS Nanoparticle Necklaces with functionalized Dendronized Polymers. *Small* **2006**: 11 1314-1319.
- Roman Gajda, Andrzej Katrusiak.; Electrostatic Matching versus Close-Packing Molecular Arrangement in Compressed Dimethyl Sulfoxide (DMSO) Polymorphs. *J.Phys.Chem.B* **2009**: 113 2436-2442.

- Thelma Serrano, Idalia Gomez, Rafael Colas, Jose Cavazos.; Synthesis of CdS nanocrystals stabilized with sodium citrate. *Eng.Aspects* **2009**: 338 20-24.
- G.Z. Wang, W.Chen, C.H. Liang, Y.W.Wang, G.W. Meng and L.D. Zhang.; Preparation and characterization of CdS Nanoparticles by ultrasonic radiation. *Inorganic Chemistry Communications* **2001**: 4(1) 208-210.
- Qiyu Yu and Chun-Yan Liu.; Study of Magic Size –Cluster Mediated formation of CdS Nanocrystals: Properties of the Magic-Size Clusters and Mechanism Implications. *J. Phys. Chem.* **2009**: 113 12766-12771.
- X. Y. Liu, *J. Phys. Chem. B* **2001**: 105, 11550-11558
- Cheng Jin, Zou Xiao-Ping, Song Wei-Li, Cao Mao-Sheng, Su, Yang Gang-Qiang, Lu Xue-Ming, Z Fu-Xue, Zhang.; Shape-Controlled Synthesis and Related Growth Mechanism of Pb(OH)<sub>2</sub> Nanorods by Solution-Phase Reaction. *CHIN. PHYS. LETT.* **2010** 27 (5); 057302-1 to 057302-4.
- Jin Cheng, Xiaoping Zou, Weili Song, Xiangmin Meng, Yi Su, Gangqiang Yang, Xueming Lü, Fuxue Zhang and Maosheng Cao.; Effects of concentration of chloride anion on the morphology and microstructure of precipitates from lead nitrate solutions. *CrystEngComm*, **2010**, 12, 1790-1794.
- Xiao-Ling Shi, Mao-Sheng Cao, Jie Yuan, Quan-Liang Zhao, Yu-Qing Kang, Xiao-Yong Fang, and Yu-Jin Chen.; Nonlinear resonant and high dielectric loss behavior of CdS/ $\alpha$ -Fe<sub>2</sub>O<sub>3</sub> heterostructure nanocomposites. *Appl. Phys. Lett.* **2008**, 93, 183118.

## References Chapter 6

1. Prashant V. Kamat.; Photophysical, Photochemical and Photocatalytic aspects of metal nanoparticles. **2002**. *J.Phys.Chem. B* 106; 7729-7744.
2. Kittel C.; Introduction to Solid State Physics. Seven Edition. *Jon Wiley & Sons*. **1996**.
3. Thelma Serrano, Idalia Gomez, Rafael Colas, Jose Cavazos.; Synthesis of CdS nanocrystals stabilized with sodium citrate. *Eng.Aspects* **2009**: 338 20-24.
4. V.P. Singh, R.S. Singh, G.W. Thompson, V. Jayaraman, S. Sanagapalli, V.K. Rangari. Characteristics of nanocrystalline CdS films fabricated by sonochemical methods for solar cell applications. *Solar Energy Materials and Solar Cells* **2004**: 81 293-303

5. G.Z. Wang, W.Chen, C.H. Liang, Y.W.Wang, G.W. Meng and L.D. Zhang.; Preparation and characterization of CdS Nanoparticles by ultrasonic radiation. *Inorganic Chemistry Communications* **2001**: 4(1) 208-210.
6. S. Martinez, T. Serrano, I. Gomez, A. Hernandez.; Synthesis and Characterization of CdS nanoparticles by microwave irradiation. *Bol.Soc.Esp.Ceram.* **2007**: 46(2) 97-101.
7. C. Unni, Daizy Philip, S.L. Smitha, K.M. Nissamudeen, K.G. Gopchandran.; Aqueous synthesis and characterization of CdS, CdS:Zn<sup>2+</sup> and CdS:Cu<sup>2+</sup> quantum dots. *Spectrochimica Acta Part A:Molecular and Biomolecular Spectroscopy* **2009**: 72(4) 827-832.
8. Manoj E. Wankhede, Santosh K. Haram.; Synthesis and Characterization of Cd- DMSO Complex Capped CdS Nanoparticles. *Chem.Mater* **2003**: 15 1296-1301.
9. N. Revaprasadu, S.N. Mlondo.; Use of metal complexes to synthesize semiconductor nanoparticles. *Pure Appl.Chem.* **2006**: 78(9) 1691-1702.
10. P.K. Khanna and Narendra Singh.; Light emitting CdS quantum dots in PMMA: Synthesis and optical studies. *J. of Luminescence* **2007**: 127 474-482.
11. Junjie Zhu, Miaogao Zhou, Jinzhong Xu and Xuehong Liao.; Preparation of CdS and ZnS nanoparticles using microwave irradiation. *Materials Letters* **2001**: 47, 25-29.
12. Liang Li, Huifeng Qian and Jicun Ren.,; Rapid synthesis of highly luminescent CdTe nanocrystals in the aqueous phase by microwave irradiation with controllable temperature. *Chem. Commun.*, **2005**, 528–530
13. Aslan K.; Saccharide Sensing Using Gold and Silver Nanoparticles. **2004**. *Journal of Fluorescence* 14(4); 391.
14. Gedes, C.; Luminescent Blinking from Noble-Metal Nanostructures: New Probes for Localization and Imaging. **2003**. *Chemical Physics Letters*. 380; 269-272.
15. Mock J.J. et al.; Shape effects in plasmon resonance of individual colloidal silver nanoparticles. **2002**. *Journal of Chemical Physics*. 116(15); 6755-6759.
16. Gammon D.; Optical Studies of Single Quantum dots. **2002**. *Physics Today*. 55(10); 36-42.
17. S.Nieto et al. Nanoscaled Science and Engineering for Sensing: Quantum Dots Fluorescence Quenching for Organic NO<sub>2</sub> Sensing. **SPIE 2004**.
18. Xiaohu Gao.; Moleccular profiling of single cells and tissue specimens with quantum dots. **2003**. *Trends in Biotechnology* 21(9): 271

19. Salata, OV. Applications of nanoparticles in biology and medicine. *Journal of Nanobiotechnology*, **2004**, 2, 1-6.
20. Penn S.H., Nanoparticles for bioanalysis. **2003**. *Chemical Biology* 7; 609-615.
21. Xiaohu Gao.; In vivo cancer targeting and imaging with semiconductor quantum dots. **2004**. *Nature Biotechnology*. 22(8); 969.
22. Collinson P.O., Are Troponins Confusing. **Nov.2003**. *Heart* 89(11); 1285.
23. Plenbani, M.; Quality Specifications for biochemical markers of myocardial injury. **2004**. *Clinica Chemica Acta* 346 65-72.
24. Lee, I., Luo, X., Cui, X.T., Yun, M., Highly sensitive single polyaniline nanowire biosensor for the detection of immunoglobulin G and myoglobin, *Biosensors and Bioelectronics* (2010), doi:10.1016/j.bios.2011.01.001
25. Wu, W.; Bian, Z.; Wei Wang, P.; Wang, W.; Zhu, J. PDMS gold nanoparticle composite film-based silver enhanced colorimetric detection of cardiac troponin. *Sensors and Actuators B*, **2010**,147, 298–303.
26. You JJ, Austin PC, Alter DA , Ko DT, Tu JV. Relation between cardiac troponin I and mortality in acute decompensated heart failure. *American Heart Journal* 2007; 153:462-470.
27. Hentschel D. M., Aviles R. J., Topol E. J., Lauer M. S. Troponin T Levels and Acute Coronary Syndromes. *New Engl J Med*. 2002; 347:1722-1723.
28. Antman EM. Decision Making with Cardiac Troponin Tests. *New England Journal of Med* 2007; 346: 2079-2082.
29. Antman E M, Tanasijevic MJ, Thompson B, Schactman M, McCabe CH, Cannon CP, Fischer GA, Fung AY, Thompson C, Wybenga D, Braunwald E. Cardiac-Specific Troponin I Levels to Predict the Risk of Mortality in Patients with Acute Coronary Syndromes. *New England Journal of Med* 1996; 335(18): 1342-1349.
30. Olatidoye AG, Wu AHB, Feng YJ, Waters D. Prognostic role of troponin T versus troponin I in unstable angina pectoris for cardiac events with meta-analysis comparing published studies. *J. of Cardiology* 1998; 81(12): 1405-1410.
31. Brus LE. Electron-electron and electron-hole interactions in small semiconductor crystallites: The size dependence of the lowest excited electronic state. *The Journal of Chemical Physics* 1984; 80: 4403-4403.
32. Apple, F.; Maturen, A. J.; Mullins, R. E.; Painter, P. C.; Pessin-Minsley, M.; Webster, R. A.; Spray Flores, J.; DeCresce, R.; Fink, D. J.; Buckley, P. M.; Marsh, J.; Ricchiuti, V.;

- Christenson, R.H. Multicenter Clinical and Analytical Evaluation of the AxSYM Troponin-I Immunoassay to Assist in the Diagnosis of Myocardial Infarction. *Clinical Chemistry*, **1999**, *45*, 206–212
33. Braunwald E. Biomarkers in Heart Failure. *New England Journal of Medicine* **2008**; *358*:2148-2159.
34. Dong Hwan Choi, Seok Ki Lee, Young Kyoung Oh, Byeong Woo Bae, Sung Dong Lee, Sanghyo Kim, Yong-Beom Shin, Min-Gon Kim. A dual gold nanoparticle conjugate-based lateral flow assay (LFA) method for the analysis of troponin I. *Biosensors and Bioelectronics* **25 (2010)** 1999–2002
35. Ferrer Torres, Edmy J., Zayas, F., La Torre, E. and Miguel E. Castro. Fluorescence response of CdS nanoparticles to serum of cardiac patients: towards the development of a real time sensor for heart failure detection. *Puerto Rico Health Science Journal* September 2009.

## APPENDIX A

---

### Active Learning Activities in Nanotechnology

#### General Methodology

Students performed the activity to have hands on experience on the topics presented in the laboratory lectures. No indication or instructions were given as to what amounts to mix of the different reactants, or how to operate the instruments they were going to use. After each activity, the students had the opportunity to spend a five to ten minute period just talking about their accomplishments and what they learned in nanotechnology.

In this activity the students were introduced to concepts such as chemical kinetics, nanoparticles, light absorption, clusters and effects of nanoparticles size. For the synthesis of gold nanoparticles they prepared different citrate solutions (1.92mM, 3.84 mM, 5.76 mM and 7.68 mM) using the stock solution previously prepared. They also prepared KAuCl<sub>4</sub> 1.92 mM solution. Then they mixed the citrate and gold solution in four beakers and allowed it to stabilize (change of color). Finally they measured the absorbance of each sample on a UV-Vis spectrometer. Then they compared the absorbance with the particle size.

An example of the module use in the general chemistry laboratory is presented below:

## **Title: Reaction Kinetics; Gold nanoparticle synthesis**

### **I. Objective:**

Relate the synthesis of gold nanoparticles with the kinetics of a reaction.

### **II. Introduction:**

Chemistry is concerned with change. Chemical reactions convert substances with well-defined properties into other materials with different properties. Much of our study of chemical reactions is concerned with the formation of new substances from a given set of reactants. However, it is equally important to understand how rapidly chemical reactions occur.

The area of chemistry that is concerned with the speeds, or rates, of reactions is called chemical kinetics. Chemical kinetics is a subject of broad importance. It relates, for example, to how quickly a medicine is able to work, to whether the formation and depletion of ozone in the upper atmosphere are in balance, and to industrial problems such as the development of catalysts to synthesize new materials. Factors that affect the reaction rates are concentrations of reactants, temperature, surface area of solid reactants and catalyst.

In this experiment we will study the effect of temperature and reactant concentration in the synthesis of gold nanoparticles. Nanoparticles are defined as particles of less than 100nm in diameter, that exhibit new or enhanced size-dependent properties compared with larger particles of the same material. Nanoparticles are of interest because of the new properties such as chemical reactivity and optical behaviour that they exhibit compared with larger particles of the same materials. Nanoparticles have a range of potential applications: in cosmetics, textiles and paints, and medicine.

### III. Materials:

#### Reactants



#### Equipments

50 mL beaker or Erlenmeyer flask

1" or 1 cm stir bar

Stirring hotplate

Droppers

### IV. Procedure:

1. Add the select amount of  $\text{HAuCl}_4$  to a 50.0 mL beaker or Erlenmeyer flask on a stirring hot plate. Add a magnetic stir bar and bring the solution just to a boil.
2. To the boiling solution, add the select amount of a 1% solution of trisodium citrate dihydrate,  $\text{Na}_3\text{C}_6\text{H}_5\text{O}_7 \cdot 2\text{H}_2\text{O}$ . The gold solution gradually forms as the citrate reduces the gold (III).
3. Repeat steps 1 and 2 with two more different amounts of reactants.
4. Study the presence of a colloidal suspension by the reflection of a laser beam from the particles.
5. Obtain the UV-VIS spectra for each prepared solution.

## References

1. Drexler Erick K.; *Bull Sci & Soc.* **2004** Feb 24(1): 21-27
2. Smarglick P.; *Nature.* **2002** Aug 15; 418(6899); 4-6
3. Ballew NL.; *Chem.Biol.* **2004** Jan 11(1); 1-2.
4. Lehmpuhl, David W.; *J.Chem.Educ.* **2003.** 80:466.
5. Felder R.M. and Brendt R.; *J.Chem. Educ.* **2003.** Fall 37(4): 282-283
6. Mohamed, Mona B. Volkov V., Link S., El Sayed, Mostafa A.; *Chem. Phys. Let.* **2000** Feb (317) 517-523.
7. Wilcoxon J.P., Martin, J.E.; *J.Chem.Phys.* **1998** 108(21) 9137-9143.
8. Chen, Yit-Tsong, Tamkang; *J. Sci. & Eng.* **2002** 5(2) 99-106.
9. Heinz, W.F. and Hoh, J.H.; *J.Chem.Educ.* **2005** May 82(5) 695-703
10. Hipps, K.W. and Scudiero, L.; *J.Chem.Educ.* **2005** May 82(5) 704-710.